Highly-resolved satellite remote sensing based land-use change inventory yields weaker surface albedo-induced global cooling

Authors: Xiaohu Jian[1], Xiaodong Zhang[1,*], Xinrui Liu[1], Kaijie Chen[1], Tao Huang[2], Shu Tao[1], Junfeng Liu[1], Hong Gao[2], Yuan Zhao[2], Ruiyu Zhugu[1], Jianmin Ma[1]

Affiliations:

[1]Laboratory for Earth Surface Processes, College of Urban and Environmental Sciences, Peking University, Beijing 100871, PR China

[2]Key Laboratory for Environmental Pollution Prediction and Control, Gansu Province, College of Earth and Environmental Sciences, Lanzhou University, Lanzhou 730000, PR China

[*]**Corresponding author:** Xiaodong Zhang (zhangxd2020@pku.edu.cn)

Abstract

Land-use change (LUC) is ranked as the second anthropogenic source of climate change after fossil fuel burning and yields negative albedo-induced radiative forcing (ARF). This cooling effect has been assessed using low spatiotemporally resolved LUC datasets derived from historical statistical data with large uncertainties. Herein, we implement a satellite remote sensing derived highly resolved LUC dataset into a compact earth system model and reassess the global and regional surface ARF by LUC from 1983 to 2010 relative to 1750. We find that the magnitude of negative ARF obtained from the present study is lower by 20% than that estimated by the Intergovernmental Panel on Climate Change, implying a weaker cooling effect. The result reveals that the global LUC-induced surface albedo change may not significantly slow down global warming as was previously anticipated. Sub-Saharan Africa made the largest net proportion to the magnitude of global ARF (39.2%), due to substantial land use conversions, typically the conversion from forest to other vegetation lands, which accompany with higher surface albedos. The most remarkable land cover changes occurred in East and Southeast Asia, which dominated the changes in global ARF in recent decades. Based on major land cover types in these two regions, we infer that vegetation lands exert a most vital effect on global ARF variation.

1. Introduction

Anthropological activities that have effectuated global climate change can be primarily categorized under greenhouse gas emissions, the emissions of aerosols, and land use change (LUC) (IPCC AR6, 2021). LUC in different temporal and spatial scales varies rapidly from local to global scales, with significant ramifications for the climate system, and is one of the key drivers of global climate change (Feddema et al., 2005; Cai et al., 2004; Foley et al., 2005; Houghton et al., 2012; Zhu et al., 2019). LUC accounts for 13%–20% of the total anthropogenic carbon emissions from the 1990s to the 2010s, and 20% in the 1980s and 1990s (Houghton et al., 2012), ranking as the second source of anthropogenic climate change after fossil fuel combustion (Andrews et al., 2017). The influence of LUC on climate change is primarily manifested in two critical processes: the radiation/energy interface between the surface and the atmosphere and the changes in the carbon source/sink. LUC affects climate by emitting or absorbing greenhouse gases in the atmosphere, modifying the carbon cycle within the climate system. In other words, the effect of LUC on climate balance involved in understanding how changes in land use (such as afforestation, urbanization, or land restoration) affect the climate system's energy balance through biogeochemical and biogeophysical processes. These processes drive carbon sequestration and emissions and surface albedo change (Gries et al., 2019). LUC also modifies the albedo and roughness of the underlying surface, altering the surface heat budget. By functioning as a carbon sink through carbon reduction-oriented land management, LUC plays a pivotal role in the sequestration of carbon (IPCC AR6, 2021). Such LUC-induced carbon sinks are crucial for compensating emissions from other carbon sources, such as fossil fuel energy, transportation, and housing, that continue to emit carbon dioxide.

The extent of the influence of LUC on the climate system and energy balance is often measured in terms of radiative forcing (RF) (Andrews et al., 2017; Andrews et al., 2020; Ramanathan et al., 1975; Bonan et al., 2008; Betts et al., 2000; Ward et al., 2014). The primary effect of RF on climate change is through a temperature feedback mechanism (Sherwood et al., 2015). While the effects of LUC on climate balance have been extensively studied from the biogeochemical perspective (Foley et al., 2005; Houghton et al., 2012; Vose et al., 2004; Gries et al., 2019), knowledge gaps still remain in the understanding of LUC-induced climate forcing from the biogeophysical perspective. This is partly due to the lack of extensive investigations

62 in the long-term effects of LUC-induced climate forcing prediction and uncertainties in this
63 field (IPCC AR6, 2021). Immediate impacts may be different from those observed over
64 decades or centuries. Long-term temporal studies that track these changes are limited. The
65 commonly held belief is that the change in surface albedo associated with LUC has a negative
66 forcing globally, leading to a cooling effect and functioning as a carbon sink. However, the
67 magnitudes of negative forcing vary between -0.15 W m^{-2} and -0.6 W m^{-2} in different studies
68 spanning the pre-industrial to industrial era (IPCC AR3, 2001; Myhre et al., 2003; Hansen et
69 al., 2004; Betts et al., 2007; Forster et al., 2007; Pongratz et al., 2009; Ward et al., 2014; Li et
70 al., 2016; Jiao et al., 2017). The Intergovernmental Panel on Climate Change (IPCC) AR3
71 report (2001) (IPCC AR3, 2001) adopted -0.25 ± 0.25 W m^{-2} as the global average RF due to
72 surface albedo change. This value has been revised in subsequent reports to -0.15 ± 0.10 W
73 m^{-2} (IPCC AR6, 2021). The magnitude of negative RF induced by surface albedo (hereafter
74 referred to as ARF) obtained from other studies appears to be greater than the IPCC adopted
75 value (Fig. 1). In AR3 of the IPCC, the scientific understanding of LUC-induced ARF was
76 deemed "very low". Due to the limited number of studies and the uncertainty of historical land
77 cover (LC) changes, IPCC AR6 (2021) assigns these values a medium confidence level. A
78 substantial proportion of the uncertainties in LUC and ARF can be attributed to the lack of high
79 spatiotemporal resolution in LUC data and sufficient supports by measurements (Gong et al.,
80 2013; Winkler et al., 2021; Jian et al., 2022). Recently, numerous high-resolution remote
81 sensing datasets have been used to develop highly resolved LUC datasets (Gong et al., 2013;
82 Winkler et al., 2021). Modern satellites are equipped with sensors that offer high spatial
83 resolution, allowing for the detailed mapping of land-use changes. This level of detail is
84 essential for identifying specific types of land-use changes, such as deforestation, urban
85 expansion, or agricultural intensification, each of which has different impacts on radiative
86 forcing. These remote sensing-based datasets reveal that LUC has affected as much as one-
87 third of the world's land area in just six decades (1960–2019), roughly four times greater than
88 the estimates from long-term land change assessments conducted previously (Winkler et al.,
89 2021). It is interesting to know if and to what extent recently developed remote sensing-based
90 global land use (LU) change data with very high spatial-temporal resolution from a climate
91 perspective and potentially low uncertainty could improve the estimation of LUC-induced
92 global and regional climate forcing.

93   In the present study, we reassessed the LUC forced ARF by incorporating a high-
94 resolution (5 km×5 km) satellite remote sensing measured LUC dataset into a compact earth
95 system model (see Methods) and evaluate the contributions from various LUC and LU types
96 in different regions/countries to global ARF, aiming to provide a more precise and
97 measurement-based estimate of regional and global ARF.

98

2. Materials and Methods

2.1. OSCAR Model

101   OSCAR v2.4 (Gasser et al., 2017), a compact model of global biogeochemical cycles, is
102 used to investigate the effect of LUC-induced changes in surface albedo on global RF. OSCAR
103 is not spatially resolved but country and region-based. It is a nonlinear box model incorporating
104 as many key climate components and modules as possible, such as LU change and aerosol
105 physics-chemistry feedback. The model was designed to simulate long-term trends in earth
106 system change rather than seasonal and interannual variations in the earth system. OSCAR is
107 also a parametric model in which several parameters required to calculate RF are calibrated on
108 (or input from) complex climate models. Model uncertainties are assessed by Monte Carlo
109 ensembles, including input LUC, surface albedo, and other model parameters. In the present
110 study, we have assigned a 5% uncertainty in OSCAR modeled ARF based on LUC data
111 uncertainty. The uncertainty of the LUC data is subject to its accuracy (82.81%, Liu et al.,
112 2020). We examined the response of modeled ARF to the 5% uncertainty by increasing the
113 uncertainty to 10% and 15%. The differences of simulated mean ARF between 5% and 10%
114 and 15% were only 0.23% and 0.47%, respectively. Further details, advantages of OSCAR
115 model, and the motivations to use OSCAR model in our ARF simulations are presented in
116 Supplementary Text 1.

117

2.2. Updated Global LUC Data

119   The OSCAR's capability to simulate LU change-induced RF is one of its strengths. To
120 assess the combined effects of human activities on the carbon-climate system (Hurtt et al.,
121 2011), the model employs the LU Harmonization (LUH1) LUC dataset developed under IPCC-
122 AR5. The results show a smooth transition of annual changes in LUC, suggesting that approach

123   and data sources adopted to derive LUH1 (Supplementary Text 2) likely missed some

124   important characteristics of LU transitions, resulting in a substantial uncertainty in the modeled

125   LUC-induced RF. Although LUH1 was recently updated to LUH2 with a spatial resolution of

126    $0.25° \times 0.25°$ latitude/longitude (Hurtt et al., 2020), in the present study, we chose the Global

127   Land Surface Satellite-Global LC dataset (GLASS-GLC) (Liu et al., 2020) to replace the LUH1

128   inventory with coarse spatial resolution in the OSCAR model to capture the temporal-spatial

129   variations of LUC adequately. GLASS-GLC was developed using 5 km×5 km resolution

130   GLASS (Global Land Surface Satellite) climate data records from 1982 to 2015. Although both

131   LUH and GLASS-GLC provide annual LUC, compared to previous LUC products, such as

132   LUH1 and LUH2, GLASS-GLC based on satellite remote sensing has greater consistency, a

133   higher spatial resolution, and many LU types. Compared to LUH1 dataset derived based on

134   historical statistics and census data combining with the History Database of the Global

135   Environment (HYDE) model and the Global Land-use Model (GLM) (Hurtt et al., 2011), the

136   GLASS-GLC dataset uses the Google Earth Engine (GEE) platform with the latest version of

137   GLASS CDRs (climate data records) from 1982 to 2015 (Liu et al., 2020) to obtain a more

138   reliable land use inventory.

139   It should recognize the differences between the satellite-derived land cover classifications

140   (GLASS-LUC) and the land use classifications (LUH1) and reconcile the differences. Table

141   S1 list mapping categories of the LUH1 and GLASS-GLC. GLASS-GLC considers seven LUC

142   classes, including cropland, forest, grassland, shrubland, tundra, barren land, and snow/ice,

143   with an overall accuracy of 82.81%. Although the GLASS-GLC data source also include urban

144   areas, these small areas are not straightforward to be distinguished at the 5 km×5 km resolution

145   as compared to other LUCs (Liu et al., 2020). Besides, while urban expansion could contribute

146   to climate warming (Ouyang et al., 2022), our previous work (Jian et al., 2022) has explored

147   the impact of urbanization on China's ARF and found that the impact of urban sprawl on

148   China's ARF is very small (0.59%) and hence can be neglected, although China has

149   experienced the world's most rapid urbanization since the 1980s (Yang et al., 2013), due to

150   considerably smaller area of urban land than the other selected 6 LU categories. Likewise, the

151   urban land also exerts a little effect on ARF from a global perspective. Therefore, urban areas

152   were not taken into consideration in this study. The LUC data are available for download at

https://doi.org/10.1594/PANGAEA.913496. Noted that, although the updated GLASS-GLC was extended to 2015, given that some of parameters and variables in OSCAR v2.4 were only available up to 2010, we performed OSCAR simulations from 1982 to 2010.

We further compared the GLASS-LUC derived ARF in the OSCAR model to the modeling result using another satellite remote sensing derived LUC, namely, the MODIS LUC data (Moderate Resolution Imaging Spectroradiometer, 2014, https://modis.gsfc.nasa.gov/). Given that the MODIS-LUC data is only available from 2001 to 2023, we replaced the GLASS-GLC by MODIS LUC data from 2002 to 2010 in the OSCAR model. During this period, the accumulated RF simulated by the OSCAR in the globe using the MODIS LULC and the GLASS-GLC data are 0.0165 Wm^{-2} and 0.0157 $W\ m^{-2}$, respectively, indicating only a 5% difference of between the RFs using the two LUC datasets derived from satellite remote sensing. Sun et al. (2022) compared the applications of six LULC products in the identification of LUCs in Northwestern China. Their results revealed, while the GLASS-GLC and MODIS (MCD-12Q1) were not superior to other four products, these two datasets were of most temporal and spatial consistency.

The OSCAR model does not take the surface roughness length into account. The surface roughness affects primarily on turbulent exchange of heat and air mass between the underlying surface and air, which may indirectly alter surface radiation fluxes via changing sensible and latent fluxes under a heat balance status (Andrews, 2012). This characteristic can significantly influence RF largely via its association with surface albedo. Given that the OSCAR introduces directly the surface albedo, it is expected that excluding the roughness length would not perturbate RF prediction significantly.

2.3. Sensitivity Analysis

To illustrate the influence of LUC-induced albedo change on the global RF, we chose five LU types that have dominated the global LUCs over the past four decades: cropland, desert, forest, grassland, and shrub. Considering that, for many satellite-derived land-use classification products, overall classification accuracies range between 70% and 90%, implying that misclassifications can lead to an uncertainty of 10% to 30% in land-use area estimates (Gong

182   et al., 2013), we carried out extensive sensitivity experiments by reducing each LU transition

183   area by 20% within five major LU types (cropland, desert, forest, grassland, and shrub). These

184   sensitivity evaluations aimed to examine the relative significance and contribution the LU

185   conversion and transition among different LU types to the ARF. Among them, each LU type

186   is converted to the rest four LU types, thereby accounting for total 20 LU transitions and

187   sensitivity experiments. However, in the original OSCAR inventory, there were only inter-

188   conversions between cropland and other land types, and no conversions between desert, forest,

189   grassland, and shrub. Table S2 presents these 20 LU transitions from 1982 to 2010. To facilitate

190   analysis and refine the effect of LUC on ARF, the world has been divided into nine regions.

191   These regions include East and Southeast Asia (including China), Europe, Latin America, the

192   Near East and North Africa, North America, Oceania, Russia, Sub-Saharan Africa, and South

193   Asia (Fig. 2). Table S3 presents the surface albedos for the five LU types in each nation and

194   the nine regrouped global regions. Between the OSCAR LUH1-LUC inventory and the

195   GLASS-GLC inventory, Fig. S1 and Table S4 compare annual changes in the area of each LU

196   type from 1982 to 2010 in the globe and the nine regions. There are distinct differences between

197   the two LUC inventories. The causes of these differences and two simulation results are

198   discussed in Supplementary Text 2. By performing OSCAR simulations with a low

199   spatiotemporally resolved OSCAR LUH1-LUC inventory (Scenario 1) and a high

200   spatiotemporally resolved GLASS-GLC inventory (Scenario 2), respectively, we also set up

201   two model scenarios for sensitivity experiments. Detailed results of sensitivity analysis are

202   presented in Table S5

203

204   **2.4 Methods of comparing ARF results for two datasets**

205   The percentage changes in annual ARF between the two scenarios are estimated using the

206   following equation:

207    $ARF_F = (ARF_{S2} - ARF_{S1}) \times 100\% / ARF_{S1}$ (1)

208   where ARF_F, ARF_{S1}, and ARF_{S2} represent the percentage changes in ARF and ARF values from

209   model scenarios 1 and 2, respectively.

210

211   **2.5. Disturbance Capacity Analysis and Effective Area**

212   We conducted comprehensive sensitivity experiments on OSACR simulations to analyze

213 the impact of each of the 20 LU conversions on ARF globally and across of the nine regions.

214 We consider the conversion from each of the five LU types to the remaining four LU types,

215 resulting in 20 LU conversion types (Table S2). In these sensitivity experiments, we introduce

216 a disturbance capacity (DC, %) that determines the magnitude of the ARF change induced by

217 the 20 LU conversions in the region of interest. The DC is defined as follows:

218
$$
\begin{cases}
\Delta RF_{ij} = \overline{RF_i} - \overline{RF'_{ij}}, \\[2em]
DC_{ij} = \dfrac{\Delta RF_{ij}}{\sum_{j=1}^{20} |\Delta RF_{ij}|} * 100\%.
\end{cases}
\tag{2}
$$

219 where, $\overline{RF_i}$ represents mean ARF in region i averaged from 1983 to 2010. We reduce the jth

220 LU conversion in region i by 20% and define resulted ARF in region i as RF'_{ij} in each year.

221 Its mean from 1983 to 2010 is defined as $\overline{RF'_{ij}}$. Expression (2) can also be considered as a

222 statistical formula for determining the relative significance or the contribution of ARF induced

223 by a particular LU conversion to the total ARF change across all regions and LU conversion

224 types. For example, the sensitivity experiment for grassland to cropland conversion in region i

225 (13th sensitivity experiment or LU conversion) was conducted by multiplying the area

226 converted from grassland to cropland by 0.8, indicating a 20% reduction in the grassland to the

227 cropland transition area. The changes (or response) of ARF in region i perturbed by a 20%

228 reduction in the jth LU conversion area ΔRF_{ij} were then used to estimate DC_{ij} (Eq. 2).

229   We also examine net LU conversion among the five LU types, where net LU conversion

230 is defined as the difference between a pair of LU conversions. For instance, the net conversion

231 from grassland to cropland (13th LU conversion, Table S2) and from cropland to grassland (3rd

232 LU conversion, Table S2) is calculated as the area converted from grassland to cropland minus

233 the area converted from cropland to grassland, also referred to as the net two-way conversion.

234 This adjustment reduces the total LU conversions in the sensitivity experiment from 20 to 10.

235 The DC for the ten net LU conversion areas is definable as follows:

$$\begin{cases} A_{a\leftrightarrow b}^t = A_{a\rightarrow b}^t - A_{b\rightarrow a}^t, \\\\ DC_{a\leftrightarrow b} = \dfrac{DC_{a\rightarrow b}}{|DC_{a\rightarrow b}|} * \left(\dfrac{|DC_{a\rightarrow b}| + |DC_{b\rightarrow a}|}{2} \right). \end{cases} \tag{3}$$

where $A_{a\leftrightarrow b}^t$ is the area of net LU transition, a and b indicate the conversion from LU type a to type b, respectively, $A_{a\rightarrow b}^t$ and $A_{b\rightarrow a}^t$ are the transition areas from LU type a to LU type b, and from LU type b to a. The superscript t denotes a specific year between 1982 and 2010. $DC_{a\leftrightarrow b}$ represents the disturbance capacity of net conversion between paired LUs, and $DC_{a\rightarrow b}$ and $DC_{b\rightarrow a}$ are the DC of LU conversion $a \rightarrow b$ and $b \rightarrow a$, respectively. After the DC of LU conversion is determined, we estimate an effective area (EA) (see main text), which is defined here as the cumulative area of six net LU conversions, given by

$$\begin{cases} \alpha_{ik} = \dfrac{DC_{ik}}{\sum |DC_{ik}|}, if\ |DC_{ik}| \geq 1\%, \\\\ \alpha_{ik} = 0, if\ |DC_{ik}| < 1\%, \\\\ A_{it}^e = \sum_{k=1}^{10} \alpha_{ik} * A_{ikt}. \end{cases} \tag{4}$$

where DC_{ik} represents the DC in the *kth* net LU conversion type affecting ARF in region i. The ratio of DC_{ik} to the absolute value of total DC_{ik}, defined by in Eq. (4), can also be viewed as the proportion of different net LU conversions to the global EA (Table S6). A_{it}^e denotes the EA in year t and region i. A_{it}^e indicates the area of the *kth* net LU conversion type in year t and region i. Consequently, the EA measures the extent of a LU conversion area that significantly impacts the change in ARF. In calculating the EA, we first exclude net LU conversions with $|DC| > 1\%$, then sum up these $|DC|$ values ($\Sigma|DC|$) and finally divide the DC of each net LU conversion with $|DC| > 1\%$ by $\Sigma|DC|$ (Eq. 4). Table S6 presents the correlation coefficients and significance tests of the EAs. According to Eq. 4, once the DC is obtained, the EA area can be estimated, which defines the converting areas of the 10 net land conversion types between 1982 and 2010 divided by their respective absolute DCs. The results explain the change in ARF from 1983 to 2010 (Supplementary Text 3).

2.6. Quantifying the Contribution of Regional LU Transition to Changes in Global ARF and Effective Area

The changes in ARF due to LU conversion in a region from 1983 to 2010 can be simply defined as the differences in ARF between 1983 and 2010. First, we considered the ARF change in any region across the globe as:

$$\Delta ARF_{LU\_all} = RF_i'^{\,2010} - RF_i'^{\,1983}. \tag{5}$$

where, $RF_i'^{\,2010}$ and $RF_i'^{\,1983}$ denote the ARF in *the ith* region in the S2 scenario using the GLASS-GLC inventory in 2010 and 1983, respectively. To remove the effect of LU conversion on ARF, we reduced the transition area of each LU type from 20% to 100% in the 20 sensitivity experiments, meaning no occurrence of LU transition. Second, we introduced $RF_{i,j}^{2010}$ and $RF_{i,j}^{1983}$ to represent the ARF in the ith region induced by the jth LU transition in the S2 scenario in 2010 and 1983, so their differences are as follows:

$$\Delta ARF_{LU\_ind} = RF_{i,j}^{2010} - RF_{i,j}^{1983}. \tag{6}$$

This can be regarded as the changes in ARF induced by other 19 conversion types for the jth LU conversion during this period. The changes in ARF subject to any LU conversion in any of the nine regions can be written as:

$$\delta_F = \Delta ARF_{LU\_all} - \Delta ARF_{LU\_ind}. \tag{7}$$

In other words, δ_F indicates the net effect of regional LU transition on ARF. Finally, the contribution of ARF from any region and any LU conversion to the changes in global ARF is defined as:

$$C_{ARF} = \frac{\delta_f}{ARF_{global}^{2010} - ARF_{global}^{1983}}. \tag{8}$$

here, ARF_{global}^{2010} and ARF_{global}^{1983} are global ARF in 2010 and 1983 from model scenario 2. Their difference is constant (0.0364 W m^{-2}).

The contribution of regional EAs to the global EA is simply estimated by Eq. 9:

282 $$C_{EA} = \alpha_{i,k} \times \frac{\sum_{n=1}^{28} \frac{EA_{n,i}}{\sum_i^9 EA_{n,i}}}{28}.$$ (9)

283 where, $i = 1, 2, \ldots 9$ denotes nine regions, $n = 1, 2, \ldots 28$ is the number of years from 1983 to

284 2010 and $\alpha_{i,k}$ is defined in Eq. (4).

285   The contribution of two-way LU conversions to the changes in global ARF is defined by

286 Eq. 10:

287 $$C_{LV}^k = \sum_{i=1}^{9} \sum_{j=1}^{8} C_{ARF}^{i,j}.$$ (10)

288 where, $k = 1,2\ldots5$ denotes five LU types, $i = 1, 2,\ldots,9$ denotes nine regions, and $j = 1,2,\ldots,8$

289 indicate paired two-way LU transitions. Taking cropland as an example, the one-way

290 transitions between cropland to the remaining four LU types are the transitions from cropland

291 to forestland, grassland, desert, and shrubland. The other way includes transitions from

292 forestland, grassland, desert, and shrubland to cropland. So the two-way transition includes

293 eight LU conversions.

294

295 **3. Results**

296 **3.1. Response of Global RF to Perturbed Albedo**

297
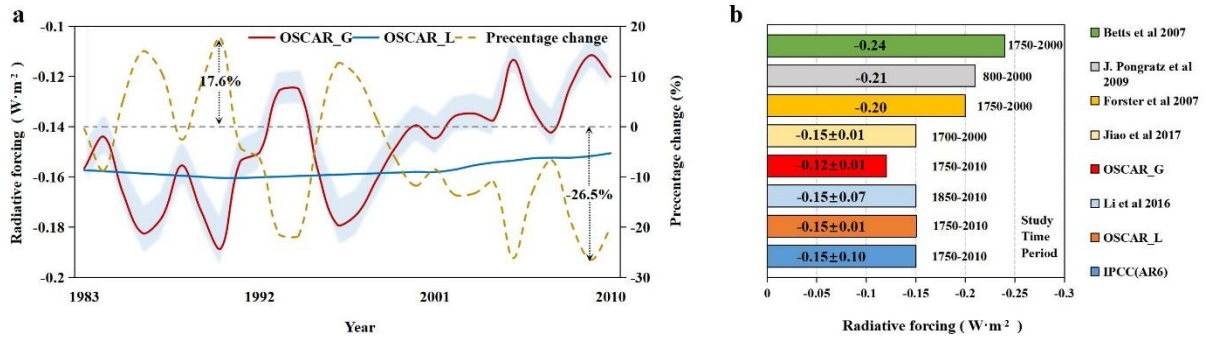
298 **Figure 1.** Annual RF (W m^{-2}) due to albedo change and ARF percentage change (%) and different ARF

299 derived from previous studies. (a) OSCAR-modeled annual RF due to the albedo change and ARF

300 percentage change between the two model scenarios S1 and S2 from 1983 to 2010 derived from coarse

301 resolution LUH1-LUC inventory (solid blue line, see 'Methods') and GLASS-GLC inventory (solid red line,

302 see Methods). The annual ARF of 1983 through 2010 from both model scenarios is relative to the baseline

303 year of 1750. Two-tailed T-Test yields a p-value of 0.025 (<0.05), indicating the statically significant

304 difference between OSCAR-G and OSCAR-L data series. Pale blue shading indicates the uncertainty

305 interval estimated from Monte Carlo simulations. Dashed yellow line stands for a percentage change in ARF

306 from the two scenarios. (b) ARF from present (red color bar) and previous (other color bars) studies from

307 different time period. However, the results of the studies covering the year 2010 all point to the result of

308 2010.

309

310   To examine the extent of the changes in global RF subject to the altered surface albedo

311 derived from LU transition from 1983 to 2010, we compared the ARF using the coarse

312 resolution LU Harmonization v1-LU Change [LUH1-LUC inventory (OSCAR_L, model

313 scenario S1)] extending from 1750 to 2010 and the fine resolution Global Land Surface

314 Satellite-Global LC dataset [GLASS-GLC inventory (OSCAR_G, model scenario S2)] in

315 OSCAR simulations. It is noted that the annual ARF derived from the model scenario 1 was

316 relative to the baseline year of 1750. The annual ARF derived from the model scenario 2 was

317 also relative to 1750 but we replaced LUH1-LUC with GLASS-GLC after 1982. Fig. 1a depicts

318 the OSCAR-simulated annual global ARF subject to the two model scenarios. From 1983 to

319 2010, annual ARFs derived from the two LUC scenarios demonstrated upward trend. In

320 contrast, the ARF in the S1 simulation (solid blue line) displays a smoother variation and a

321 weaker increase with a linear trend of 0.0003 (P-value < 0.01). The smooth transition from

322 historical LUC estimates to future projections in the LUH1-LUC results in such gradual

323 changes in the ARF. In contrast, the ARF in the S2 simulation (solid red line) displays strong

324 interannual fluctuations and a more rapid increase with a linear trend of 0.0018 (P-value $<$

325 0.01). The dashed brown line indicates the resulting ARF_F ranges from -26.5% (2009) to 17.6%

326 (1990). Globally, both scenarios produce negative forcing, consistent with previous estimates

327 (IPCC AR6, 2021; Li et al., 2016). As aforementioned, even though we only replaced the

328 coarse resolution LUH1-LUC inventory with the fine resolution GLASS-GLC inventory, the

329 ARF in the OSCAR is predicted since the industrialization era in the 1750s, the same as the

330 IPCC AR6. This suggests that both scenario simulations utilized the same LUH1-LUC data

331 before 1982. Consequently, significant annual and decadal changes in ARF have occurred over

332 the past few decades, alongside rapid and remarkable global variations in LUC. The significant

333 differences in the ARF between the two scenarios can be attributed to different data sources

334 and approaches applied to derive LUH1-LUC and GLASS-GLC. The former was developed

335   from a combination of historical statistics, population census data, HYDE, and GLM models.

336   Because the time covered by this inventory are outside the period of satellite observations,

337   large uncertainties in LUH1-LUC have been recognized (Hurtt et al., 2020). A higher

338   resolution land use dataset can ensure interannual consistency and comparability of the LUC,

339   and enables the accurate estimation of the rate and mode in LUC (Gong et al., 2013; Liu et al.,

340   2020), which can capture more detailed LUC and LU transitions. Recent reports indicate that

341   the global LUC is four times larger than previously estimated (Winkler et al., 2021). The

342   differences between the two LUC datasets are shown in Supplementary Text 2, Text 4, Table

343   S4, and Fig. S1.

344   Previously estimated global ARF with coarse resolution LUC data has been subject to

345   several concerns. According to the IPCC Assessment Reports, the global RF induced by LUC

346   from pre-industrial times to the present due to changes in land albedo is approximately -0.15

347    $\pm\ 0.10$ W m^{-2}, indicating that ARF plays a cooling role (IPCC AR6, 2021). Considering that

348   radiative forcing is often accumulated from the past, the differences of ARF from the two

349   inventories occurred mostly in final year, namely 2010. Our OSCAR simulation under scenario

350   1 using a LUH1-LUC inventory yielded the same negative ARF value of -0.15 W m^{-2} as

351   reported by the IPCC (Fig. 1b). Using coarse resolution and historical statistics-based LUC

352   data, additional studies have also obtained ARF results with great uncertainties. As depicted in

353   Fig. 1b, all previous studies yielded stronger negative ARFs than the IPCC's estimate, with the

354   negative ARF reaching as low as -0.24 W m^{-2} (Betts et al., 2007). However, our estimation

355   subject to scenario 2 yields an ARF of -0.12 ± 0.01 W m^{-2}, which is only half of that reported

356   by Betts et al (2007). The result suggests that the global LUC-induced surface albedo change

357   may not be acting as anticipated to slow down the global warming.

358

359   **3.2. Contribution of Regional LUC to Global ARF**

360

361
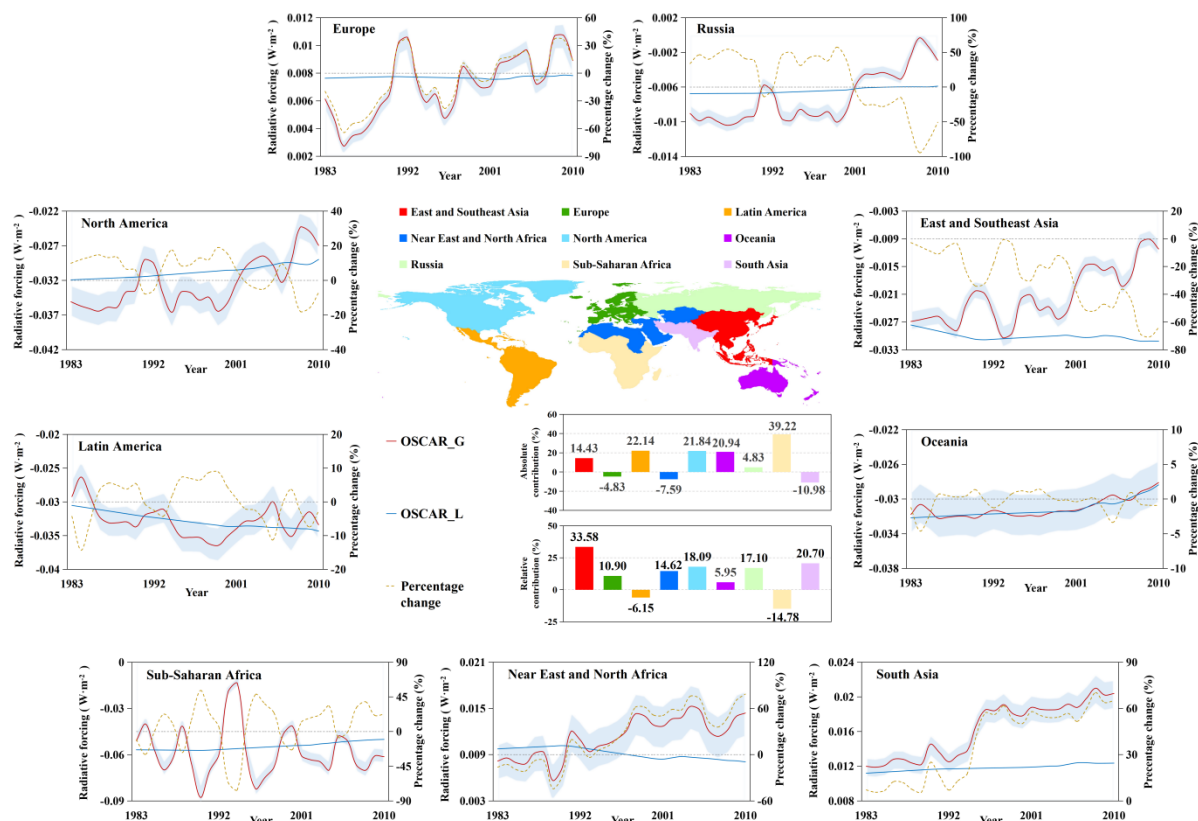
Figure 2. Annual RF (W m^{-2}) due to the albedo change and ARF percentage change between the two model scenarios S1 and S2 from 1983 to 2010 derived from LUH1-LUC inventory (solid blue line) and GLASS-GLC inventory (solid red line) in nine regions across the globe. The pale blue shading indicates the uncertainty interval estimated from Monte Carlo simulations. The dashed brown line stands for the percentage change in the annual ARF$_{i-F}$ between the LUH1-LUC inventory (ARF$_{i-S1}$) and GLASS-GLC inventory (ARF$_{i-S2}$), in which *i* represents regions, respectively, including East and Southeast Asia, Europe, Latin America, Near East and North Africa, North America, Oceania, Russia, Sub-Saharan Africa, and South Asia. The first bar chart illustrates the absolute contribution of different regions to the global albedo-induced RF, and the second bar chart displays the relative contribution of different regions to the global albedo-induced RF changes. The nine color bars represent different regions, as indicated by the color legend above the colored sectional map.

373

In recent decades, LUC has been subject to significant spatial heterogeneity across the globe. To investigate the magnitude of the response of global ARF to continental/regional LUC since the 1980s, we divided 113 countries and territories in OSCAR into nine regions. Each of the nine regions encompasses a specific number of countries and territories (Table S3). The

mean ARF value for each of the nine regions was calculated by averaging the ARFs over the countries and territories in each of the nine regions. The colored sectional map in the center of Fig. 2 indicates the nine regions. In addition, the annual variation of the ARF subjected to GLASS-GLC (W m^{-2}, solid red line, scaled on the left Y-axis) and its percentage change (%, dashed brown line, scaled on the right Y-axis) in each of these regions are illustrated in the nine-line charts of Fig. 2. Below the sectional map are two bar charts depicting the absolute and relative contributions of the nine regions to the global ARF. Correspondingly, the total contribution is defined as the proportion of the mean ARF of each nine regions to the global mean ARF from 1983 to 2010. The relative contribution is defined as the proportion of the change in ARF in each of the nine regions to the change in global ARF between 1983 and 2010. In addition, the OSCAR-simulated ARFs in each region derived from LUH1-LUC (solid blue line, scaled to the left on the Y-axis) are displayed in the line charts. Herein, OSCAR predicts ARFs by incorporating fine-scale variations, as opposed to the LUH1-LUC-derived ARFs with smoothing variations; GLASS-GLC, on the other hand, displays more pronounced annual fluctuations. In East and Southeast Asia and Near East and North Africa, the simulated ARFs derived from the two LUC datasets exhibit opposite trends from 1983 to 2010, indicating that LUC data substantially influence regional and continental ARFs.

As evident from the bar charts below the sectional map, among the nine regions, Sub-Saharan Africa, with a mean ARF of -0.06 W m^{-2} on average from 1983 to 2010, made the largest net contribution (39.2%) to the global mean ARF. The significant contribution from Sub-Saharan Africa is attributable to its large desert area of 697.37 Mha with a high albedo (Table S3) and pronounced LU conversions among vegetated LU types (Fig. S2 and Table S4). South Asia had a mean ARF of 0.02 W m^{-2} from 1983 to 2010. This region had an absolute negative contribution of -10.98% to the global mean ARF averaged over the nine regions, most likely because of rapidly expanding croplands (226.93 Mha) with low albedo associated with the Green Revolution (Pingali et al., 2012; Liu et al., 2021; Huang et al., 2022) (Fig. S2 and Table S4). East and Southeast Asia, Europe, Latin America, Near East and North Africa, North America, Oceania, and Russia contributed 14.43%, -4.83%, 22.14%, -7.59%, 21.84%, 20.94%, and 4.83% to the global mean ARF, respectively.

Although East and Southeast Asia made a moderate absolute contribution to the global mean ARF compared to other regions, this region experienced the largest LU change between

1982 and 2010. This was characterized by the highest ARF change (0.017 W m^{-2}), comprising the most significant relative contribution (33.58%) to the global ARF change. Such a contribution can be attributed to the massive LC changes brought on by afforestation and the management of land desertification during this time period (Liu & Xin, 2021; Imai et al., 2018; Zhang et al., 2016), which led to a decrease in surface albedo. In contrast, deforestation in Sub-Saharan Africa in recent decades (Keenan et al., 2015) promoted rapid shrub growth (Atsri et al., 2018; Mograbi et al., 2015), resulting in a rise in albedo. Consequently, this region has the largest negative contribution to the global ARF change, at −14.78%, promoting a cooling effect on the global climate. Similarly, the deforestation in Latin America caused by the conversion of forest to cropland and pastureland in recent decades (Armenteras et al., 2021; Hansen et al., 2013; Nogueira et al., 2019; Davidson et al., 2012) also led to the increase in surface albedo, thus, contributing −6.15% to the global ARF change between 1983 and 2010.

The differences (percentage change, %) in regional ARF between the two scenarios for the nine regions are depicted by the brown dashed lines (scaled on the right Y-axis) in the line charts of Fig. 2. Except for Europe, the Near East and North Africa, and South Asia, where the annual ARFs are stronger than those derived from LUH1-LUC, the percentage changes in most regions exhibit the opposite phase of the ARFs predicted by OSCAR using GLASS-GLC. In East and Southeast Asia, for instance, the ARF derived from the S1 model scenario decreased from −0.028 W m^{-2} in 1983 to −0.031 W m^{-2} in 2010, indicating a reinforced cooling effect. In contrast, the ARF derived from the S2 scenario using the GLASS-GLC inventory exhibits the change from −0.027 W m^{-2} in 1983 to −0.011 W m^{-2} in 2010, indicating an attenuated cooling effect. The result suggests again that the LUH1-LUC inventory does not capture the change in LUC in East and Southeast Asia since the 1980s. Other details are presented in Table S7. Similar variations and trends of GLASS-GLC-driven ARFs can be observed in Russia, North America, and Oceania, where the negative ARFs exhibit rising trends from 1983 to 2010, indicating once again the declining negative ARF values and weakening cooling effect. In South Asia, the average percentage change in ARF between the two scenarios is the highest, at 37.30%. Moreover, Europe, the Near East and North Africa, and South Asia yielded positive ARFs. The increasing ARF trends indicate an intensification of the warming effect in these regions during this period. Sub-Saharan Africa experienced the greatest negative ARF values and fluctuations in both model scenarios. We found that the ARF from the S1 scenario extended

440   from −0.057 W m^{-2} in 1983 to −0.050 W m^{-2} in 2010. The ARF from the S2 scenario dropped

441   from −0.051 W m^{-2} in 1983 to −0.061 W m^{-2} in 2010. These results illustrate that the LUH1-

442   LUC data attenuates the cooling effect in Sub-Saharan Africa, whereas the GLASS-GLC

443   inventory enhances the cooling effect, demonstrating once again that the LUC data with

444   significantly different resolutions and sources could alter the conclusions in the evaluation of

445   LUC-induced climate forcing. Further details are provided in Supplementary Text 4 and Table

446   S7.

447

448   **3.3. Effective Area of LU Conversion and Interannual ARF Variations**

449
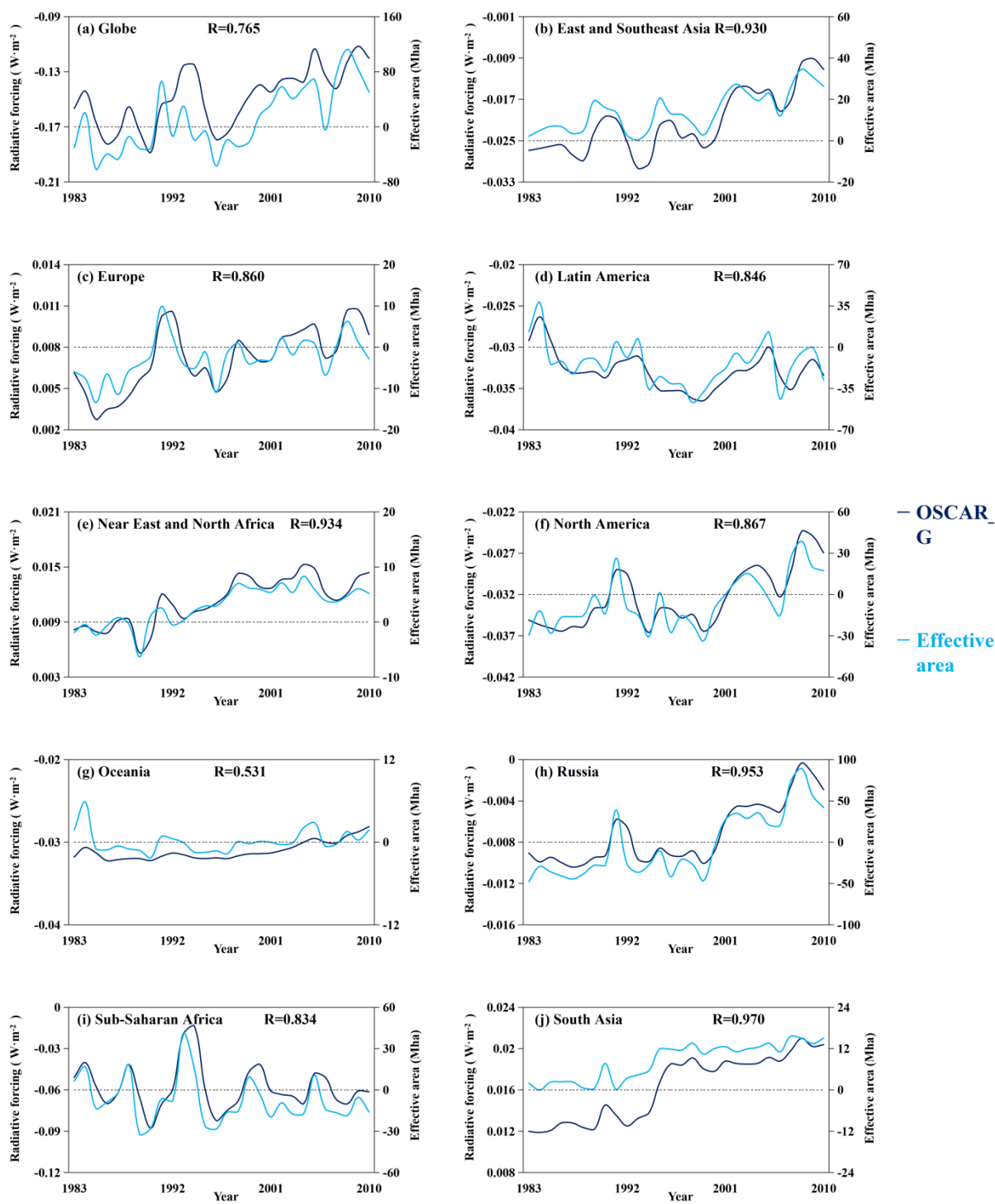
Figure 3. Annual RF (W m^{-2}) due to surface albedo change in model scenarios 2 from 1983 to 2010 derived from GLASS-GLC inventory (solid black line) and effective area (solid blue line) in the globe and nine regions. (a) Globe; (b) East and Southeast Asia; (c) Europe; (d) Latin America; (e) Near East and North Africa; (f) North America; (g) Oceania; (h) Russia; (i) Sub-Saharan Africa; (j) South Asia. Correlation

455 coefficients between the ARF and effective area are marked in the figures. The effective area measures the

456 extent of the area of all net LU conversion contributing to the change in ARF (see Methods).

457

458   We designed 20 sensitivity experiments to examine the contribution of LU conversion

459 among the five LU types to the variation in ARF from 1982 to 2010 (Methods, Table S2). We

460 introduced a disturbance capacity (DC, %), and an effective area (EA, see Eq. 4 in Methods)

461 to explain the changes in ARF caused by the size of LU conversion areas. Here, DC (%)

462 quantifies the extent of LU conversion that may considerably impact the change in ARF. The

463 EA is the sum of six net LU conversions that quantifies the extent of LU conversion

464 contributing to the change in ARF. In the sensitivity experiments, we reduced the area of LU

465 transition by 20% for each LU conversion (Gong et al., 2013). The model combines the ARF

466 results from 20 sensitivity experiments with the LUC for each target region. Further details are

467 provided in Methods and Supplementary Text 3. We also analyzed the rate and magnitude of

468 annual ARF fluctuations associated with EAs in the world and nine regions between 1983 and

469 2010. The details are presented in Supplementary Text 5 and Figs. S3–S12.

470   Figure 3 depicts the annual ARF (scaled on the left Y-axis) and EA (scaled on the right

471 Y-axis) in the globe and nine selected regions. As seen, the global annual ARF, which is the

472 sum of the ARFs in the nine regions based on OSCAR simulations, is stronger than regional

473 ARF due to the larger scale of global land cover change (Table S4 and Fig. S1) and stronger

474 albedo changes. The correlation coefficient between the ARF and EA in the globe is 0.765 (*P*-

475 value < 0.01), indicating that the net LU conversion area in the globe explains 59% of the

476 global ARF variation. In this instance, the global EA consists of a cumulative area of six net

477 LU conversion types. The percentage of individual LU conversions to the global EA is

478 presented in Table S6 and Fig. S13. As shown in Fig. S13a, the interannual fluctuations of the

479 EA (blue solid line) agree well with that of the transition area from the grassland-to-forest land

480 (red dashed line). Together with the grassland to cropland transition, these two LU transitions

481 contribute the most to the global LU transition, accounting for 52.5% of the total EA worldwide.

482 Such significant LU conversions have been attributed to grassland degradation (Bardgett et al.,

483 2021; Andrade et al., 2015; Aune et al., 2018; Berangere et al., 2018), such as the expansion

484 of croplands in the US, which reduced prairie grasslands (Lark et al., 2020). Since the surface

albedo of grassland is greater than that of forest and cropland (Edouard et al., 2010; Jackson et al., 2008), grassland degradation could be considered a major contributor to the increase in global ARF since the mid-1990s (Fig. 3a). This increasing ARF is crucial to the attenuation of the cooling effect of the global negative ARF from -0.15 W m^{-2} to -0.12 W m^{-2}. In East and Southeast Asia, the correlation coefficient between ARF and EA is 0.930 (*P*-value < 0.01), indicating that the EA explains 86% of the ARF change in this region. In particular, the interannual fluctuation of the EA agree well with the LU transition from cropland to forestland (green dashed line, Fig. S13b), followed by the transition from grassland to forestland (red dashed line). Afforestation plays a key role in the ARF changes in East and Southeast Asia, including grassland to forest, shrub to forest, and cropland to forest. These three LU transitions account for 68.6% of total EA in this region. Previous reports have indicated that the forest area in Southeast Asia has been decreasing in recent decades (Hansen et al., 2013; Achard et al., 2002; Estoque et al., 2019) and has suffered from a net loss of 1.6 million ha yr^{-1} (0.6% yr^{-1}), thus, reducing the region's forest cover from 268 million ha in 1990 to 236 million ha in 2010 (Stibig et al., 2014). However, China has expanded the world's largest afforested area since the late 1980s and had the world's largest artificial forest area in 2008, comprising approximately 62 million hectares (National Forest Resource Inventory Report, 2009; http://www.fao.org/forestry/fra/fra2010/en/, 2010; Zhang et al., 2015). Consequently, the forest cover in East and Southeast Asia has expanded accordingly. Given the low albedo of forested land (Igusky et al., 2008) and the forest land expansion over the past four decades (Zhang et al., 2016; Peng et al., 2014), we observed a decreasing albedo and more positive ARF in these regions. In Latin America, the correlation between ARF and EA is 0.846 (*P*-value < 0.01). As shown in Fig. S13d, the annual variation of the EA nearly overlaps with the transition zone between grassland and forest land. This LU transition contributes 77.4% to the EA in Latin America, thereby playing a significant role in the ARF in this continent. In recent decades, forest areas in Latin America have experienced a dramatic decline (Global Forest Resources Assessment, 2020), partly due to forest wildfires (ARAGÃO et al., 2010; Escobar et al., 2019) and the transition from forest lands to pastureland under the significantly rising global demand for agricultural products (such as meat and soybeans) in this region. Correspondingly, remarkable deforestation (Armenteras et al., 2019; Bullock et al., 2020) and conversion of forest to grassland have been observed (Andela et al., 2017). Spanning almost

516 15 years (1990 to 2005), Latin America has been reported to have lost 7% of its forests (Da

517 Ponte et al., 2015). This transition resulted in an increase in albedo and a decrease in ARF in

518 Latin America (Fig. 3d).

519 The correlation coefficient between the ARF and the EA in Sub-Saharan Africa is 0.834

520 (P-value < 0.01). The EA in this region consists of the cumulative area of five net LU

521 conversions (Table S6). The conversion between forestland and shrubs made the largest

522 contribution (48.9%) to the total EA. Sub-Saharan Africa is home to most of the world's

523 tropical grassy ecosystems (grasslands and savannas), comprising ~33.5% of Africa's landmass

524 (Parr et al., 2014). In recent years, the forest area in Sub-Saharan Africa has decreased

525 (Carherine et al., 2013), accompanied by an increase in savanna (including shrubs) (Atsri et al.,

526 2018; Gaillard et al., 2018). As depicted in Fig. 3i and Fig. S13i, declining forestland in Sub-

527 Saharan Africa consistently produces negative ARF, despite annual fluctuations.

528 In South Asia, the correlation coefficient between ARF and EA is 0.97 (P-value < 0.01),

529 with the EA including the cumulative area of six net LU conversions (Table S6). Of these LU

530 conversions, cropland-related LU transitions contributed up to 81.4% to the total EA. This

531 region of Asia has experienced the most successful Green Revolution since the late 1960s (Liu

532 et al., 2021), and India is one of the largest producers of agricultural commodities (FAOSTAT:

533 Food and agricultural data, 2017; Teluguntla et al., 2015), with more than half of its territory

534 used for cropland. Since the 1980s, the continuous expansion of cropland in South Asia (Hinz

535 et al., 2020) has led to a decrease in albedo, increasing ARF (Fig. 3j and Fig. S13j). Further

536 discussions on EA in Europe, the Near East and North Africa, North America, Oceania, and

537 Russia, as shown in Fig. S13, are presented in Supplementary Text 6.

538

539 **3.4 Response of Global ARF Change to Regional LUC Area and LU Conversion**
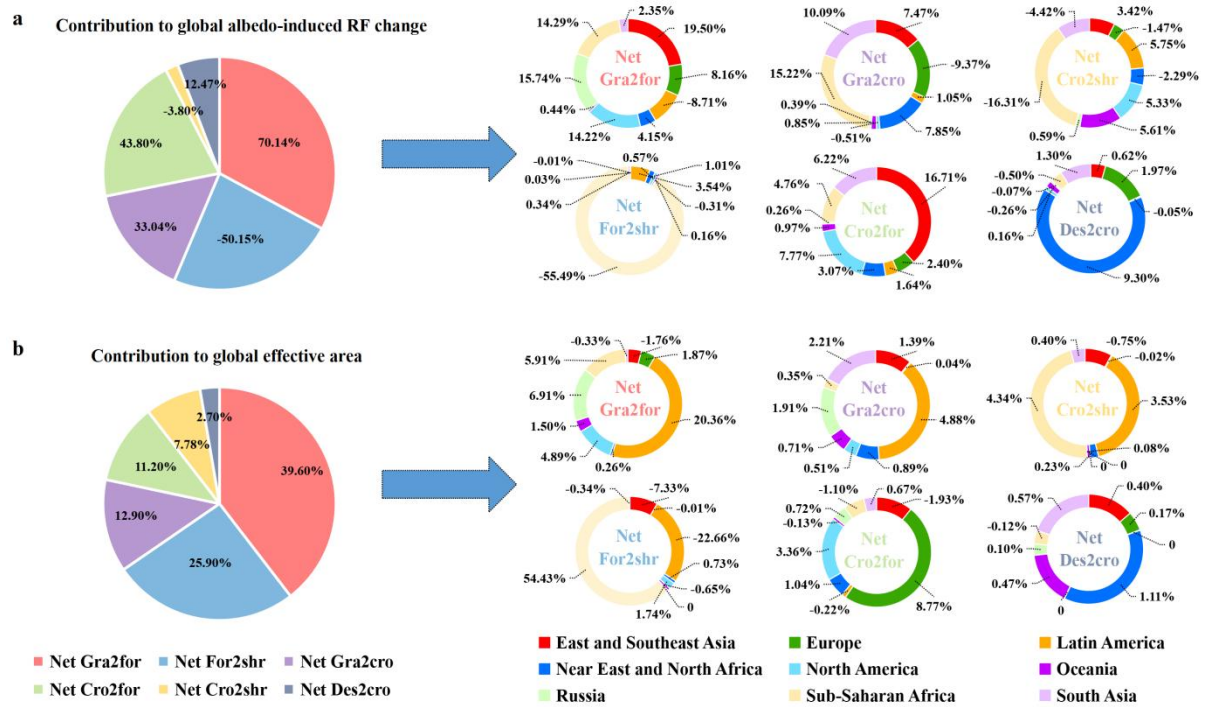
Figure 4. Contribution of six net LU conversion types in nine regions (|DC| > 1%) to the change in global ARF and EA globally and nine regions. (a) Pie charts on the left panel show the contribution of six LU conversion types in nine regions to the change in global ARF, including grassland to the forest (orange), forest to shrubs (light blue), grassland to cropland (light purple), cropland to the forest (light green), cropland to shrubs (light yellow), and desert to cropland (light gray). Donut charts on the right panel show the contribution of each of the six net LU conversion types in each of the nine regions to the change in global ARF. Among the nine regions, East and Southeast Asia are colored red, Europe deep green, Latin America deep yellow, Near East and North Africa deep blue, North America blue, Oceania purple, Russia green, Sub-Saharan Africa yellow, and South Asia purple gray. The coefficient of variation (CV) is ±5%. (b) Contribution of six LU conversions (|DC| > 1%) in the nine regions to global EA.

To quantify the contribution of each LU transition in each region to the changes in global ARF and EA, we estimated ARF and EA changes without LU conversion from 1983 to 2010 by reducing LU transition areas from 20% to 100% in 20 sensitivity experiments (see Methods), indicating no LU transition. Subsequently, we calculated the differences between ARF and EA changes with and without LU conversion to determine the contributions of any LU conversion in any region to the changes in global ARF and EA, as defined by C_{ARF} and C_{EA}, as described in Eqs.5–9 of Methods. The net conversion of grasslands to forests contributed 70.14% to the change in the global ARF from 1983 to 2010. During this period, the global ARF increased by

560   0.036 W m^{-2}, in line with the general upward trend. Since the albedo of grasslands is greater

561   than that of forests, we would anticipate a decrease in albedo during the transition from

562   grasslands to forests, which tends to increase the ARF. Efforts have been made to increase the

563   global forest cover through afforestation programs. However, most afforestation programs

564   have been implemented at the expense of natural vegetation, particularly grasslands, rather than

565   agricultural land (Berangere et al., 2018; Zablon et al., 2018). Globally expansive grasslands

566   were found to be suitable for future forest restoration programs to offset anthropogenic CO_2

567   emissions (Bond et al., 2016). With the updated LUC inventory with the satellite measured

568   information on a fine temporal-spatial scale, we could assess the effect of increasing forest

569   coverage on ARF with greater precision. The donut charts on the right side of Fig. 4a depict

570   the change in global ARF due to LU conversions in each of the nine regions. The results

571   indicate that grassland to forest conversion in East and Southeast Asia contributes 19.50% to

572   the change in global ARF, 8.16% from Europe, −8.71% from Latin America, 4.15% from the

573   Near East and North Africa, 14.22% from North America, 0.44% from Oceania, 15.74% from

574   Russia, 14.29% from Sub-Saharan Africa, and 2.35% from South Asia, respectively. The

575   global net conversion of forests to shrubs contributes −50.15% to the change in global ARF,

576   with individual contributions from East and Southeast Asia (0.16%), Europe (−0.01%), Latin

577   America (3.54%), Near East and North Africa (1.01%), North America (0.57%), Oceania

578   (−0.31%), Russia (0.03%), Sub-Saharan Africa (−55.49%), and South Asia (0.35%). Thus, the

579   contribution of the net conversion of forests to shrubs to the global ARF change enhanced the

580   cooling effect. The contributions from the remaining four net conversion types are shown in

581   Table S8.

582   The contributions of net conversion from grassland to forest, forest to shrubs, grassland

583   to cropland, cropland to the forest, cropland to shrubs, and desert to cropland to the global EA

584   (Eq. (4)) are 39.60%, 25.90%, 12.90%, 11.20%, 7.78%, and 2.70%, respectively, as depicted

585   in the pie charts on the left panel of Fig. 4b. The contributions of the six net conversion types

586   in each of nine regions to the global EA are displayed in donut charts in the right panel of Fig.

587   4b, providing additional information regarding the impact of regional LU conversion on the

588   variation in global ARF. For instance, the contributions of net conversion type of grassland to

589   forest in each of the nine regions to the global EA are as follows: −1.76% from East and

590   Southeast Asia, 1.87% from Europe, 20.36% from Latin America, 0.26% from Near East and

591 North Africa, 4.89% from North America, 1.49% from Oceania, 6.91% from Russia, 5.91%

592 from Sub-Saharan Africa, and −0.33% from South Asia. Additional results for the remaining

593 five types of net conversion in each of the nine regions are presented in Table S9.

3.5 Contributions of Two-way LU Conversion to Global ARF Change

595
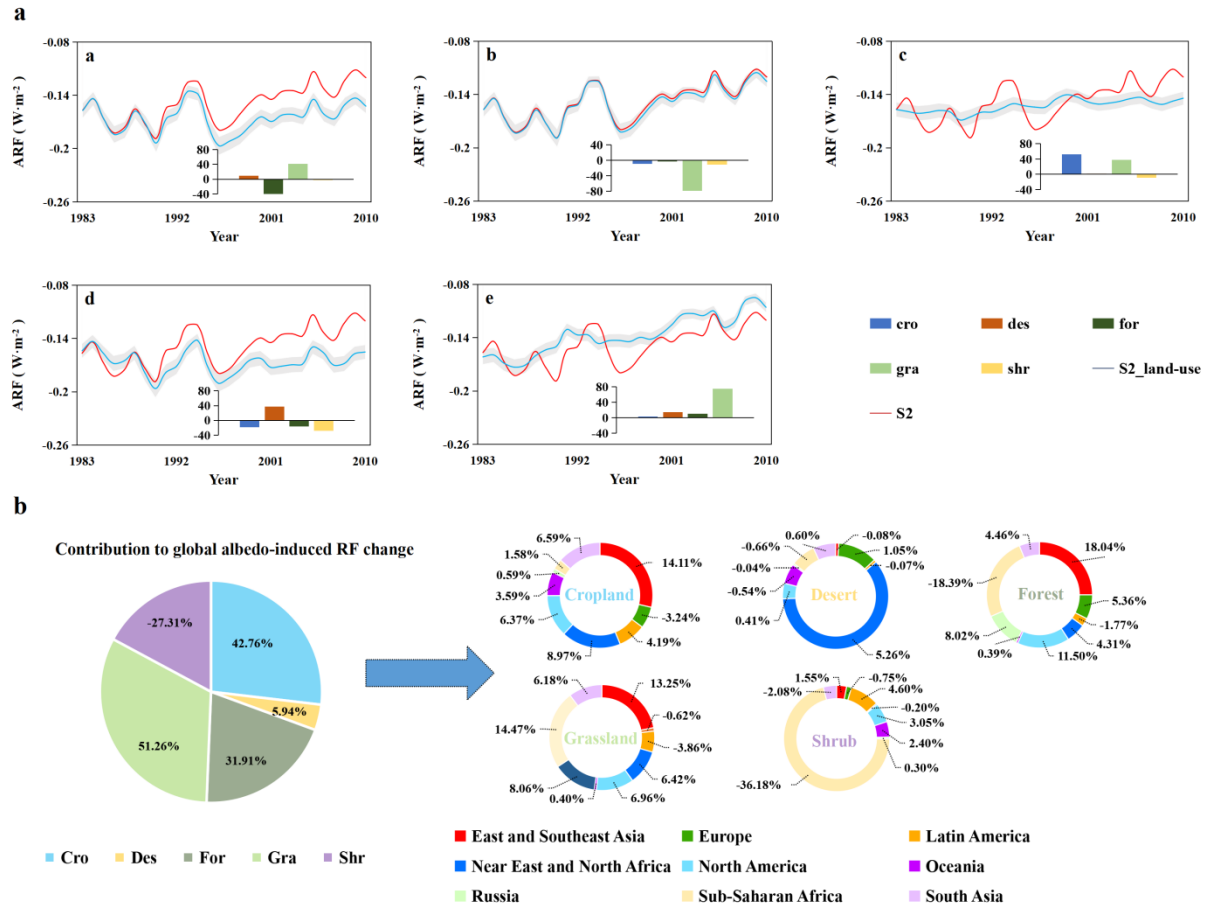
596 **Figure 5.** Changes in global ARF derived from model scenario 2 (S2) and contribution of five LU types in

597 the globe and nine regions to the change in global ARF. (a) Changes in global ARF subject to LU transition

598 from 1983 to 2010 (solid red line) and a fixed LU type without transition (solid blue line) for five LU types,

599 including croplands (cro, Fig. 5a-a), deserts (des, Fig. 5a-b), forests (for, Fig. 5a-c), grasslands (gra, Fig. 5a-

600 d), and shrublands (shr, Fig. 5a-e). The inset bar chart represents the relative contribution of the two-way

601 LU net transition between the LU of the interested and other LUs from 1983 to 2010. Taking the bar chart

602 in Fig. 5a-a as an example, the bars with different colors show the result of the two-way transition between

603 cropland and other LU types from 1983 to 2010. Positive bars represent the conversion from other LU types

604 to cropland, and negative bars indicate the transition from cropland to other LU types. Shadings in Fig. 5a-

605 a–5a-e indicate the uncertainty interval estimated by Monte Carlo simulations. (b) Contribution of five LU

606 types in each region to changes in global ARF. The pie chart on the left panel shows the contribution of five

607 LU types to the change in ARF in the globe, including cropland (light blue), desert (light yellow), forest

608 (gray-green), grassland (light green), and shrubs (light purple). Five small donut charts on the right panel

609 show the contribution of each type in each of the nine regions to changes in global ARF. The coefficient of

610 variation (CV) is ±5%.

611

612   We also set up 20 sensitivity experiments to examine the response of ARF to two-way LU

613 transition in each region. The two-way LU transition entails LU conversion from a particular

614 LU type to the remaining 4 LU types and vice versa, which accounts for eight LU conversions

615 for the five LU types in the GLASS-GLS inventory. We compare the changes in global ARF

616 driven by LU transition from 1983 to 2010 to the ARF estimated by reducing LU transition

617 areas from 20% to 100%. The 100% reduction of LU transition area means no LU transition.

618 As an illustration, Fig. 5a-a compares the change in global ARF caused by the transition

619 between cropland and the other four LUs (cropland to desert, forest, grass, and shrub, solid red

620 line) and without transition (fixed cropland, solid blue line). Marked differences can be

621 observed for both with and without the transition between croplands and other LU types. The

622 trend and annual fluctuation of ARF are consistent with the results subject to LU transition

623 (solid red line). However, under the fixed cropland (no LU transition) during this period (solid

624 blue line), the negative values of ARF change have decreased since 1990 in comparison to the

625 case with LU transition. As shown in the inset of Fig. 5a-a, the transition from grassland to

626 cropland accounts for 41.0% of the cropland transition area, while the net transition from desert

627 to cropland accounts for 9.2%. The remaining two net LU transitions occurred from croplands

628 to forests (−48.9%) and shrubs (−0.9%), respectively, implying that LU transitions from

629 croplands to other LUs account for −49.8% of the cropland transition area. By combining these

630 transition areas, the net cropland transition area was calculated to be 0.4%, indicating the

631 growth of cropland (Fig. S1). Since the transition from grasslands to croplands decreased

632 surface albedo (Table S3), the LU conversion in this instance decreases the absolute value of

633 negative ARF, thereby weakening the cooling effect.

634   Using the GLASS-GLC inventory (scenario 2), we further estimated the percentage

635 change (%) in global ARF with the transition between cropland and the other four LUs (solid

636 red line, Fig. S14a) from 1983 to 2010. During this period, the percentage changes ranged from

637 −0.6% to 28.4%, illustrating a significant upward trend. From 1998 to 2010, the annual

638 percentage change in global ARF was almost 15%, indicating that the cropland transition

639 significantly contributed to the change in global ARF. We also observed an overall increase in

640 cropland area from 1983 to 2010, as indicated by the positive accumulated cropland area in

641 Fig. S14a (solid black line, scaled to the right of the Y-axis), which is consistent with the

642 growth rate of cropland area of 0.037 Mha/yr during this period.

643 Similarly, Fig. 5a-b–5a-e illustrate OSCAR-modeled global ARF variation utilizing

644 GLASS-GLC inventory with and without LU transition of individual LU types from 1983 to

645 2010. As shown in Fig. 5a-b, the conversion of the desert to other LU types has little effect on

646 the global ARF variation, and the modeled ARF from simulations with and without LU

647 transition is nearly identical. Fig. S14b demonstrates that the percentage change in the global

648 ARF was less than 4.2% between 1983 and 2010, with a mean value of 1.7%. As illustrated in

649 the inset of Fig. 5a-b, the net transition from desert to grassland (light green bar) accounts for

650 79.1% of the total transition area, the net transition from desert to shrubs (light yellow bar)

651 accounts for 11.5% of the total transition area, and the net transition from desert to cropland

652 (deep blue bar) accounts for 8.9% of the total transition area, respectively. The percentage

653 change indicates a net decrease in a desert land, which is supported by the declining

654 accumulated area of desert land (Fig. S14b). The lack of significant differences between global

655 ARF with and without LU transition is most likely due to the smaller change in the desert area

656 over the past decades. Detailed discussions of the variations in ARF induced by forest,

657 grassland, and shrub transitions utilizing the GLASS-GLC inventory, as depicted in Fig. 5a-c–

658 5a-e are presented in Supplementary Text 7. Overall, Fig. 5a reveals an increasing trend of

659 ARF change, highlighted by attenuated negative ARF from 1983 to 2010, which suggests a

660 weakening cooling effect by the global ARF (Fig. 1).

661 Fig. 5b depicts the contribution of regional LU transactions to the change in global ARF

662 (five pie charts on the right panel of Fig. 5b). Cropland, desert, forest, grassland, and shrubs

663 contributed 42.76%, 5.94%, 31.91%, 51.26%, and −27.31%, respectively, to the change in

664 global ARF, as depicted in the pie chart on the left panel of in Fig. 5b. The donut charts on the

665 right panel of Fig. 5b illustrate the contribution of each of the five LU types in the nine regions

666 to the change in the global ARF. Taking cropland as an example, the contributions of cropland-

667 related conversions in each of the nine regions to the change in global ARF are as follows:

668 14.11% (East and Southeast Asia), −3.24% (Europe), 4.19% (Latin America), 8.97% (Near

669 East and North Africa), 6.37% (North America), 3.59% (Oceania), 0.59% (Russia), 1.58%

670 (Sub-Saharan Africa), and 6.59% (South Asia). As stated previously and depicted in the left

671 panel of Fig. 5b, the sum of the contributions from these nine regions to the global ARF change

672 is 42.76%. As a result, cropland-related LU conversion in East and Southeast Asia (primarily

673 China) made the largest contribution to global ARF variation. The results for the remaining

674 four LU types are presented in Table S5.

675

676 4. Discussion

677   By incorporating a recently developed satellite-remote sensing-based high-resolution

678 LUC dataset into the OSCAR model, we demonstrate that previous estimates of ARF derived

679 from historical statistics-based LUH1-LUC data with a coarse resolution tend to overestimate

680 the LUC driving albedo-induced cooling effect. Our revised estimate reveals that the global

681 ARF (-0.12 W m^{-2}) is lower than the value adopted by the IPCC (-0.15 W m^{-2}). Our results

682 indicate that, among the nine selected regions covering the global land area, Sub-Saharan

683 Africa made the largest net contribution (39.2%) to the global mean ARF (-0.06 W m^{-2}) owing

684 to the transition of forestland to shrubland, which result in greater surface albedo and, hence,

685 declining ARF. The latter became very significant from 1982 to 2010. East and Southeast Asia

686 also contributed significantly, following Sub-Saharan Africa, to the changes in global ARF at

687 33.6% (0.016 W m^{-2}) due to the LU conversion from the grassland to forest conversion and

688 land desertification management, which result in lower surface albedo (Table S3) and

689 increasing ARF. In line with previous researches, we demonstrate that RF induced by changes

690 in surface albedo is primarily driven by changes in vegetation (Betts et al., 2000). The

691 transformation from forest to grass, shrub, and crop, and crop to grass resulted in decrease in

692 ARF of -0.68 W m^{-2}, -0.48 W m^{-2}, -0.19 W m^{-2}, and -0.22 W m^{-2}, respectively, due to the

693 enhancement of surface albedo by the transformation from forest to these vegetation types.

694 Opposite conversions of these vegetation types to forests outweigh positive contributions to

695 ARF, indicating a rise in surface albedos and cooling effects. In addition to the magnitudes, we

696 find that the two LUC datasets developed based on different data sources, approaches, and

697 resolutions produce different ARFs, indicating that LUC data influenced considerably on

698 regional and continental ARFs.

699   Notably, the present study only predicts ARF and its change induced by surface albedo

700 subject to LUC and LU conversions but does not address RF driven by CO_2 emissions as a

701 result of carbon source-sink conversions associated with LUC and the ARF associated with the

702 LULCC-induced changes in snow cover. However, the major findings of dominant LU

703 transition patterns between forest and grassland/shrub/cropland imply CO_2 source-sink

704 transitions, which are expected to influence LUC-driven RF more strongly. On the one hand,

705 the unexpectedly weaker cooling effect of LUC observed in this study indicates that global LU

706 and LU conversion as carbon sinks since the 1980s do not significantly mitigate climate

707 warming. On the other hand, land management must be improved by increasing the capacity

708 of LUC for carbon sequestration, preserving carbon sinks, and providing renewable resources.

709 Our results show that Sub-Saharan Africa contributed the most to the forest-to-grass and forest-

710 to-shrub transition-induced global ARF, with predicted ARF values of -0.20 W m^{-2} and -0.40

711 W m^{-2}, respectively. In addition, East and Southeast Asia contribute the most to the ARF due

712 to the conversion of LU from forest to crop and crop to grass. Furthermore, Sub-Saharan Africa

713 has also been confirmed to have the highest proportion of forest-to-grass and forest-to-shrub

714 transitions, contributing to a cooling effect.

715   These findings have substantial ramifications for pertinent policy issues. Accordingly,

716 they suggest that local governments and international communities should take more action in

717 Sub-Saharan Africa to slow down or, preferably, stop deforestation and forest-to-grassland-

718 and-cropland conversion, which is a significant contributor to carbon emission enhancement

719 (Spawn et al., 2019; Pendrill et al., 2019; Chang et al., 2021). In our case, even though this LU

720 transition increases surface albedo, thereby increasing LUC-albedo–induced negative RF and

721 exerting a cooling effect, this effect is negligible compared to the increase in RF caused by

722 CO_2 emissions (IPCC AR6, 2021; Li et al., 2016; Jian et al., 2022). Therefore, the cooling

723 effect of afforestation on reducing CO_2 emissions outweighs the warming effect of the resultant

724 decrease in surface albedo. The crop-to-forest transition occurring primarily in East and

725 Southeast Asia, Europe, and the Near East and North Africa has been partially encouraged by

726 national and international cropland and water resource conservation strategies and programs,

727 resulting in ARF values of 0.09 W m^{-2}, 0.02 W m^{-2}, and 0.01 W m^{-2}, respectively. The "Grain-

728 for-Green" program in northwestern China (Wang et al., 2023), for example, impedes the

729 transition from crop to forest in East and Southeast Asia. Although the program helps improve

730 the ecological environment, from the perspective of ARF, it tends to reduce the surface albedo

731 and increase positive RF, thereby enhancing the warming effect. It is worth noting that the

732 present study did not incorporate non-radiative process and the coupling between land and

733 atmosphere, which might drive many feedback mechanisms. The significance of land

734 management in maintaining carbon sinks and providing renewable resources was also not dealt

735 with. However, this study provides additional evidence of the importance of land management

736 in influencing the carbon sinks. Optimal land management should implement integrated and

737 enforceable sustainable agriculture, climate-smart forestry, and climate-friendly land resources

738 with co-benefits and cost-efficiency.

739

740 **5. Conclusions**

741   We have improved the global and the nine regional ARF simulations using OSCAR model

742 a updated LUC dataset on a high temporal-spatial resolution. We explored the causes of ARF

743 changes in the world and nine regions across the globe by disentangling land change data for

744 20 transformation types. We also developed the concepts of DC and EA to better explain the

745 changes in ARFs. The major findings are summarized below:

746 • The magnitude of the negative ARF obtained from this study is 20% lower than previous

747   estimations, implying a weaker cooling effect. The results suggest that global LUC-

748   induced changes in surface albedo may not significantly slow global warming as

749   previously expected.

750 • Sub-Saharan Africa made the largest net contribution to the global ARF (39.2%) due to

751   significant land-use conversions, typically from forest to other vegetation land

752   accompanying with higher surface albedo. The most significant land cover changes

753   occurred in East and Southeast Asia, which dominated (33.6%) the changes in global ARF

754   in recent decades.

755 • The largest change in global ARF occurs in the net transition from grassland to forest,

756   contributing 70.14% to LUC-induced ARF. Of which, East and Southeast Asia region

757   accounts for 19.50% of the change in global ARF. The net transition from forest to shrub

made the largest negative contribution of -50.15% to the LUC-induced change in global ARF, of which Sub-Saharan Africa accounted for -55.49% to the change in global ARF.

- Vegetation lands exert a most vital effect on global ARF variation, of which grassland contributed 51.26%. Among those vegetation lands, the changes in grasslands in Sub-Saharan Africa contributed 14.47% to the global ARF variation subject to the vegetation land transition, followed by East and Southeast Asia at 13.25%.

Code availability

OSCAR v2.4 source code is available for downloading on https://github.com/tgasser/OSCAR.

Data availability

GLASS-GLC data can be accessed at https://doi.org/10.1594/PANGAEA.913496. The dataset used to generate all the results of this study is available at https://doi.org/10.5281/zenodo.14586249.

Author contributions

All authors contributed to the manuscript and have given approval of the final version. XZ coordinated and supervised the project. XZ, XJ and JM designed the present experiment, carried out modeling, and drafted the manuscript. HG, YZ and RZ collected the data. XL, KC, TH, ST and JL analyzed simulation results.

Competing interests

The authors declare that they have no known competing financial interests or personal relationships that could have appeared to influence the work reported in this paper.

Acknowledgements

We wish to thank the High-performance Computing Platform of Peking University to support extensive model simulations of this study. We acknowledge the use of OSCAR model and GLASS-GLC dataset.

Financial support

This study is supported by National Key R&D Program of China (2023YFE0112900) and the National Natural Science Foundation of China (42407134, 41991312, and 41977357).

References

Achard, F., Eva, H. D., Stibig, H. J., Mayaux, P., Gallego, J., Richards, T., and Malingreau, J. P.: Determination of Deforestation Rates of the World's Humid Tropical Forests, Science, 297, 999–1002, https://doi.org/10.1126/science.1070656, 2002.

Andela, N., Morton, D. C., Chen, L. G. Y., Werf, G. R. V. D., Kasibhatla, P. S., Defries, R. S., Collatz, G. J., Hantson, S., Kloster, S., Bachelet, D., Forrest, M., Lasslop, G., Li, F., Mangeon, S., Melton, J. R., Yue, C., and Randerson, J. T.: A human-driven decline in global burned area, Science, 356, 1356–1362, https://doi.org/10.1126/science.aal4108, 2017.

Andrade, B. O., Koch, C., Boldrini, I. I., Martin, E. V., Hasenack, H., Hermann, J. M., Kollmann, J., Pillar, V. D., and Overbeck, G. E.: Grassland degradation and restoration: a conceptual framework of stages and thresholds illustrated by southern Brazilian grasslands, Nat. & Conserv., 13, 95–104, https://doi.org/10.1016/J.NCON.2015.08.002, 2015.

Andrews, D.: An Introduction to Atmospheric Physics (2nd edition), Cambridge University Press, ISBN, 9780511800788, https://doi.org/10.1017/CBO9780511800788, 2012.

Andrews, T., Betts, R. A., Booth, B. B. B., Jones, C. D., and Jones, G. S.: Effective radiative forcing from historical land use change, Clim. Dyn., 48, 3489–3505, https://doi.org/10.1007/s00382-016-3280-7, 2017.

Andrews, T., and Forster, P. M.: Energy budget constraints on historical radiative forcing, Nat. Clim. Chang., 10, 313–316, https://doi.org/10.1038/s41558-020-0696-1, 2020.

ARAGÃO, L. E. O. C., and Shimabukuro, Y. E.: The Incidence of Fire in Amazonian Forests with Implications for REDD, Science, 328, 1275–1278, httos://doi.org/10.1126/science.1186925, 2010.

Armenteras, D., Schneider, L., and Dávalos, L. M.: Fires in protected areas reveal unforeseen costs of Colombian peace, Nat. Ecol. Evol., 3, 20–23, https://doi.org/10.1038/s41559-018-0727-8, 2019.

Armenteras, D., Dávalos, L. M., Barreto, J. S., Miranda, A., Hernández-moreno, A., Zamorano-elgueta, C., González-delgado, T. M., Meza-elizalde, M. C., and Retana, J.: Fire-induced loss of the world's most biodiverse forests in Latin America, Sci. Adv., 7, eabd3357, https://doi.org/10.1126/sciadv.abd3357, 2021.

Atsri, H. K., Konko, Y., Cuni-Sanchez, A., Abotsi, K. E., and Kokou, K.: Changes in the West African forest-savanna mosaic, insights from central Togo, Plos One, 13, e0203999, https://doi.org/10.1371/journal.pone.0203999, 2018.

Aune, S., Bryn, A., and Hovstad, K. A.: Loss of semi-natural grassland in a boreal landscape: impacts of agricultural intensification and abandonment, J. Land Use Sci., 13, 375–390,

840   https://doi.org/10.1080/1747423X.2018.1539779, 2018.

842   Bardgett, R. D., Bullock, J. M., Lavorel, S., Manning, P., Schaffner, U., Ostle, N., Chomel,
843   M., Durigan, G., Fry, E. L., Johnson, D., Lavallee, J. M., Provost, G. L., Luo, S., Png, K.,
844   Sankaran, M., Hou, X. Y., Zhou, H. K., Ma, L., Ren, W. B., Li, X. L., Ding, Y., Li, Y. H.,
845   and Shi, H. X.: Combatting global grassland degradation, Nat. Rev. Earth Environ., 2, 720–
846   735, https://doi.org/10.1038/s43017-021-00207-2, 2021.

848   Berangere, A. L., Jennifer, R. M., Charles, U., and Boris, V.: Global fire history of grassland
849   biomes, Ecol. Evol., 8, 8831–8852, https://doi.org/10.1002/ece3.4394, 2018.

851   Betts, R. A.: Offset of the potential carbon sink from boreal forestation by decreases in
852   surface albedo, Nature, 408, 187–190, https://doi.org/10.1038/35041545, 2000.

854   Betts, R. A., Falloon, P. D., Goldewijk, K. K., and Ramankutty, N.: Biogeophysical effects
855   of land use on climate: Model simulations of radiative forcing and large-scale temperature
856   change,   Agric.   For.   Meteorol.,   142,   216–233,
857   https://doi.org/10.1016/j.agrformet.2006.08.021, 2007.

859   Bonan, G. B.: Forests and Climate Change: Forcings, Feedbacks, and the Climate Benefits
860   of Forests, Science, 320, 1444–1449, https://doi.org/10.1126/science.1155121, 2008.

862   Bond,   W.   J.:   Ancient   grasslands   at   risk,   Science,   351,   120–122,
863   https://doi.org/10.1126/science.aad5132, 2016.

865   Bullock, E. L., Woodcock, C. E., Jr, C. S., and Olofsson, P.: Satellite-based estimates reveal
866   widespread forest degradation in the Amazon, Glob. Chang. Biol., 26, 2956–2969,
867   https://doi.org/10.1111/gcb.15029, 2020.

869   Cai, M., and Kalnay, E.: Impact of land-use change on climate, Nature, 427, 214,
870   https://doi.org/10.1038/427214a, 2004.

872   Catherine, B., Andreas, B. B., Francois, D., Andrea, L., Philippe, M., and Frédéric, A.:
873   Continental estimates of forest cover and forest cover changes in the dry ecosystems of
874   Africa   between   1990   and   2000,   J.   Biogeogr.,   40,   1036–1047,
875   https://doi.org/10.1111/jbi.12084, 2013.

877   Chang, J., Philippe, C., Thomas, G., Pete, S., Mario, H., Petr, H., Michael, O., Bertrand G.,
878   Daniel, S. G., Li, W., Victoria, N., Peng, S. S., Qiu, C. J., Tian, H. Q., Nicolas, V., Yue,
879   C., and Zhu, D.: Climate warming from managed grasslands cancels the cooling effect of
880   carbon sinks in sparsely grazed and natural grasslands, Nat. Commun., 12, 118,
881   https://doi.org/10.1038/s41467-020-20406-7, 2021.

883   Da, P. E., Fleckenstein, M., Leinenkugel, P., Parker, A., Oppelt, N., and Kuenzer, C.:
884   Tropical forest cover dynamics for Latin America using Earth observation data: a review
885   covering the continental, regional, and local scale, Int. J. Remote Sens., 36, 3196–3342,

886   https://doi.org/10.1080/01431161.2015.1058539, 2015.

887

888 Davidson, E. A., Alessandro, C. D. A., Paulo, A., Jennifer, K., Balch., Brown, F. I., Mercedes,
889   M. C. B., Michael, T. C., Ruth, S., Defries., Michael, K., Marcos, L., Munger, J. W.,
890   Schroeder, W., Britaldo, S. S. F., Carlos, M. S., and Steven, C. W.: The Amazon basin in
891   transition, Nature, 481, 321–328, https://doi.org/10.1038/nature10717, 2012.

892

893 Edouard, L. D., and Nathalie, D. N. D.: Climatic Impact of Global-Scale Deforestation:
894   Radiative versus Nonradiative Processes, J. Climate, 23, 97–112,
895   https://doi.org/10.1175/2009JCLI3102.1, 2010.

896

897 Escobar, H.: Bolsonaro's first moves have Brazilian scientists worried, Science, 363, 330,
898   https://doi.org/10.1126/science.363.6425.330, 2019.

899

900 Estoque, R. C., Ooba, M., Avitabile, V., Hijioka, Y., DasGupta, R., Togawa, T., and
901   Murayama, Y.: The future of Southeast Asia's forests, Nat. Commun., 10, 1829,
902   https://doi.org/10.1038/s41467-019-09646-4, 2019.

903

904 FAO, FAOSTAT: Food and agricultural data, Retrieved September 25, 2017.

905

906 Feddema, J. J., Oleson, K. W., Bonan, G. B., Mearns, L. O., Buja, L. E., Meehl, G. A., and
907   Washington, W. M.: The Importance of Land-Cover Change in Simulating Future
908   Climates, Science, 310, 1674–1678, https://doi.org/10.1126/science.1118160, 2005.

909

910 Foley, J. A., Defries, R., Asner, G. P., Barford, C., Bonan, G., Carpenter, S. R., Chapin, F.
911   S., Coe, M. T., Daily, G. C., Gibbs, H. K., Helkowski, J. H., Holloway, T., Howard, E. A.,
912   Kucharik, C. J., Monfreda, C., Patz, J. A., Prentice, I. C., Ramankutty, N., and Snyder, P.
913   K.: Global Consequences of Land Use, Science, 309, 570–574,
914   https://doi.org/10.1126/science.1111772, 2005.

915

916 Food and Agriculture Organization of the United Nations (FAO), Global Forest Resources
917   Assessment 2010, Available at: http://www.fao.org/forestry/fra/fra2010/en, 2010.

918

919 Food and Agriculture Organization of the United Nations, Global Forest Resources
920   Assessment 2020.

921

922 Forster, P., Ramaswamy, V., Artaxo, P., Berntsen, T., Betts, R., Fahey, D. W., Haywood, J.,
923   Lean, J., Lowe, D. C., Myhre, G., Nganga, J., Prinn, R., Raga, G., Schulz, M., and Dorland,
924   R. V.: Changes in Atmospheric Constituents and in Radiative Forcing. In: Climate Change
925   2007: The Physical Science Basis. Contribution of Working Group I to the Fourth
926   Assessment Report of the Intergovernmental Panel on Climate Change [Solomon, S., Qin,
927   D., Manning, M., Chen, Z., Marquis, M., Averyt, K. B., Tignor, M., and Miller, H. L.
928   Cambridge University Press, Cambridge, United Kingdom and New York, NY, USA, 2007.

929

930 Gaillard, C., Langan, L., Pfeiffer, M., Kumar, D., Martens, C., Higgins, S. I., and Scheiter, S.:
931   African shrub distribution emerges via a trade-off between height and sapwood conductivity,

J. Biogeogr., 45, 2815–2826, https://doi.org/10.1111/jbi.13447, 2018.

Gasser, T., Ciais, P., Boucher, O., Quilcaille, Y., Tortora, M., Bopp, L., and Hauglustaine, D.: The compact Earth system model OSCAR v2.2: description and first results, Geosci. Model Dev., 10, 271–319, https://doi.org/10.5194/gmd-10-271-2017, 2017.

Gong, P., Wang, J., Yu, L., Zhao, Y. C., Zhao, Y. Y., Liang, L., Niu, Z., Huang, X. M., Fu, H. H., Liu, S., Li, C. C., Li, X. Y., Fu, W., Liu, C. X., Xu, Y., Wang, X. Y., Cheng, Q., Hu, L. Y., Yao, W. B., Zhang, H., Zhu, P., Zhao, Z. Y., Zhang, H. Y., Zheng, Y. M., Ji, L. Y., Zhang, Y. W., Chen, H., Yan, A., Guo, J. H., Yu, L., Wang, L., Liu, X. J., Shi, T. T., Zhu, M. H., Chen, Y. L., Yang, G. W., Tang, P., Xu, B., Giri, C., Clinton, N., Zhu, Z. L., Chen, J., and Chen, J.: Finer resolution observation and monitoring of global land cover: first mapping results with Landsat TM and ETM+ data, Int. J. Remote Sens., 34, 2607–2654, https://doi.org/10.1080/01431161.2012.748992, 2013.

Gries, T., Redlin, M., and Ugarte, J. E.: Human-induced climate change: the impact of land-use change, Theor. Appl. Climatol., 135, 1031–1044, https://doi.org/10.1007/s00704-018-2422-8, 2019.

Hansen, J., and Nazarenko, L.: Soot climate forcing via snow and ice albedos, Proc. Natl. Acad. Sci. U.S.A., 101, 423–428, https://doi.org/10.1073/pnas.2237157100, 2003.

Hansen, M. C., Potapov, P. V., Moore, R., Hancher, M., Turubanova, S. A., Tyukavina, A., Thau, D., Stehman, S. V., Goetz, S. J., Loveland, T. R., Kommareddy, A., Egorov, A., Chini, L., Justice, C. O., and Townshend, J. R. G.: High-Resolution Global Maps of 21st-Century Forest Cover Change, Science, 342, 850–853, https://doi.org/10.1126/science.1244693, 2013.

Hinz, R., Sulser, T. B., Huefner, R., Croz, D. M. D., Dunston, S., Nautiyal, S., Ringler, C., Schuengel, J., Tikhile, P., Wimmer, F., and Schaldach, R.: Agricultural Development and Land Use Change in India: A Scenario Analysis of Trade-Offs Between UN Sustainable Development Goals (SDGs), Earth's Future, 8, e2019EF001287, https://doi.org/10.1029/2019EF001287, 2020.

Houghton, R. A., House, J. I., Pongratz, J., Werf, G. R. V. D., Defries, R. S., Hansen, M. C., Quéré, C. L., and Ramankutty, N.: Carbon emissions from land use and land-cover change, Biogeosciences, 9, 5125–5142, https://doi.org/10.5194/bg-9-5125-2012, 2012.

Huang, T., Ma, J. M., Song, S. J., Ling, Z. L., Macdonald, R. W., Gao, H., Tao, S., Shen, H. Z., Zhao, Y., Liu, X. R., Tian, C. G., Li, Y. F., Jia, H. L., Lian, L. L., and Mao, X. X.: Health and environmental consequences of crop residue burning correlated with increasing crop yields midst India's Green Revolution, Npj. Clim. Atmos. Sci., 5, 81, https://doi.org/10.1038/s41612-022-00306-x, 2022.

Hurtt, G. C., Chini, L. P., Frolking, S., Betts, R. A., Feddema, J., Fischer, G., Fisk, J. P., Hibbard, K., Houghton, R. A., Janetos, A., Jones, C. D., Kindermann, G., Kinoshita, T.,

Goldwijk, K. K., Riahi, K., Shevliakova, E., Smith, S., Stehfest, E., Thomson, A., Thornton, P., Vuuren, D. P. V., and Wang, Y. P.: Harmonization of land-use scenarios for the period 1500-2100: 600 years of global gridded annual land-use transitions, wood harvest, and resulting secondary lands, Clim. Chang., 109, 117–161, https://doi.org/10.1007/s10584-011-0153-2, 2011.

Hurtt, G. C., Chini, L., Sahajpal, R., Frolking, S., Bodirsky, B. L., Calvin, K., Doelman, J. C., Fisk, J., Fujimori, S., Goldewijk, K. K., Hasegawa, T., Havlik, P., Heinimann, A., Humpenöder, F., Jungclaus, J., Kaplan, J. O., Kennedy, J., Krisztin, T., Lawrence, D., Lawrence, P., Ma, L., Mertz, O., Pongratz, J., Popp, A., Poulter, B., Riahi, K., Shevliakova, E., Stehfest, E., Thornton, P., Tubiello, F. N., Vuuren, D. P. V., and Zhang, X.: Harmonization of global land use change and management for the period 850-2100 (LUH2) for CMIP6, Geosci. Model Dev., 13, 5425–5464, https://doi.org/10.5194/gmd-13-5425-2020, 2020.

Igusky, K.: Quantifying Albedo and Surface Temperature over Different Land Covers: Implications for Carbon Offsets, Duke University Press, 2008.

Imai, N., Furukawa, T., Tsujino, R., Kitamura, S., and Yumoto, T.: Factors affecting forest area change in Southeast Asia during 1980-2010, Plos One, 13, e0197391, https://doi.org/10.1371/journal.pone.0197391, 2018.

Intergovernmental Panel on Climate Change (IPCC), Climate Change 2001: The Scientific Basis is the most comprehensive and up-to-date scientific assessment of past, present and future climate change, Cambridge University Press, Cambridge, United Kingdom and New York, NY, USA, 2001.

Intergovernmental Panel on Climate Change (IPCC), Climate change 2021: The physical science basis, the working Group I contribution to the sixth assessment report of the intergovernmental panel on climate change, Cambridge University Press, Cambridge, United Kingdom and New York, NY, USA, 2021.

Jackson, R. B., Randerson, J. T., Canadell, J. G., Amderson, R. G., Avissar, R., Baldocchi, D. D., Bonan, G. B., Caldeira, K., Diffenbaugh, N. S., Field, C. B., Hungate, B. A., Jobbágy, E. G., Kueppers, L. M., Nosetto, M. D., and Pataki, D. E.: Protecting climate with forests, Environ. Res. Lett., 3, 044006, https://doi.org/10.1088/1748-9326/3/4/044006, 2008.

Jian, X. H., Zhang, X. D., Liu, Y. J., Liu, X. R., Chen, K. J., Wang, L. F., Li, J. X., Zhao, Y., Luo, J. M., Zhugu, R. Y., and Ma, J. M.: The Response of Radiative Forcing to High Spatiotemporally Resolved Land-Use Change and Transition From 1982 to 2010 in China, Geophys. Res. Lett., 49, e2022GL099003, https://doi.org/10.1029/2022GL099003, 2022.

Jiao, T., Williams, C. A., Ghimire, B., Masek, J., Gao, F., and Schaaf, C.: Global climate forcing from albedo change caused by large-scale deforestation and reforestation: quantification and attribution of geographic variation, Clim. Chang., 142, 463–476, https://doi.org/10.1007/s10584-017-1962-8, 2017.

Keenan, R. J., Reams, G. A., Achard, F., Freitas, J. V. D., Grainger, A., and Lindquist, E.: Dynamics of global forest area: Results from the FAO Global Forest Resources Assessment 2015, For. Ecol. Manag., 353, 9–20, https://doi.org/10.1016/j.foreco.2015.06.014, 2015.

Lark, T. J., Spawn, S. A., Bougie, M., and Gibbs, H. K.: Cropland expansion in the United States produces marginal yields at high costs to wildlife, Nat. Commun., 11, 4295, https://doi.org/10.1038/s41467-020-18045-z, 2020.

Li, B. G., Gasser, T., Ciais, P., Piao, S. L., Tao, S., Balkanski, Y., Hauglustaine, D., Boisier, J. P., Chen, Z., Huang, M. T., Li, L. Z. X., Li, Y., Liu, H. Y., Liu, H. F., Peng, S. S., Shen, Z. H., Sun, Z. Z., Wang, R., Wang, T., Yin, G. D., Yin, Y., Zeng, H., Zeng, Z. Z., and Zhou, F.: The contribution of China's emissions to global climate forcing, Nature, 531, 357–361, https://doi.org/10.1038/nature17165, 2016.

Liu, H., Gong, P., Wang, J., Clinton, N., Bai, Y. Q., and Liang, S. L.: Annual dynamics of global land cover and its long-term changes from 1982 to 2015, Earth Syst. Sci. Data, 12, 1217–1243, https://doi.org/10.5194/essd-12-1217-2020, 2020.

Liu, X. R., Zhang, X. D., Huang, Y. F., Chen, K, J., Wang, L. F., Ma, J. M., Huang, T., Zhao, Y., Gao, H., Tao, S., Liu, J. F., Jian, X. H., and Luo, J. M.: The Direct Radiative Forcing Impact of Agriculture-Emitted Black Carbon Associated With India's Green Revolution, Earth's Future, 9, e2021EF001975, https://doi.org/10.1029/2021EF001975, 2021.

Liu, X. Y., and Xin, L. J.: China's deserts greening and response to climate variability and human activities, Plos One, 16, e0256462, https://doi.org/10.1371/journal.pone.0256462, 2021.

Mograbi, P. J., Erasmus, B. F. N., Witkowski, E. T. F., Asner, G. P., Wessels, K. J., Mathieu, R., Knapp, D. E., Martin, R. E., and Main R.: Biomass Increases Go under Cover: Woody Vegetation Dynamics in South African Rangelands, Plos One, 10, e0127093, https://doi.org/10.1371/journal.pone.0127093, 2015.

Myhre, G., and Myhre, A.: Uncertainties in Radiative Forcing due to Surface Albedo Changes Caused by Land-Use Changes, J. Climate, 16, 1511–1524, https://doi.org/10.1175/1520-0442(2003)016<1511:UIRFDT>2.0.CO;2, 2003.

Nogueira, D. S., Marimon, B. S., Marimon-Junior, B. H., Oliveira, E. A., Morandi, P., Reis, S. M., Elias, F., Neves, E. C., Feldpausch, T. R., Lloyd, J., and Phillips, O. L.: Impacts of Fire on Forest Biomass Dynamics at the Southern Amazon Edge, Environ. Conser., 46, 285–292, https://doi.org/10.1017/S0376892919000110, 2019.

Ouyang, Z. T., Sciusco, P., Jiao, T., Feron, S., Lei, C., Li, F., John, R., Fan, P., Li, X., Williams, C. A., Chen, G. Z., Wang, C. H., and Chen, J. Q.: Albedo changes caused by future urbanization contribute to global warming, Nat. Commun., 13, 3800, https://doi.org/10.1038/s41467-022-31558-z, 2022.

1070
1071 Parr, C. L., Lehmann, C. E. R., Bond, W. J., Hoffmann, W. A., and Andersen, A. N.: Tropical
1072   grassy biomes: misunderstood, neglected, and under threat, Trends. Ecol. Evol., 29, 205–213,
1073   https://doi.org/10.1016/j.tree.2014.02.004, 2014.

1074
1075 Pendrill, F., Persson, U. M., Godar, J., Kastner, T., Moran, D., Schmidt, S., and Wood, R.:
1076   Agricultural and forestry trade drives large share of tropical deforestation emissions, Glob.
1077   Environ. Chang., 56, 1–10, https://doi.org/10.1016/j.gloenvcha.2019.03.002, 2019.

1078
1079 Peng, S. S., Piao, S. L., Zeng, Z. Z., Ciais, P., Zhou, L. M., Li, L. Z. X., Myneni, R. B., Yin, Y.,
1080   and Zeng, H.: Afforestation in China cools local land surface temperature, Proc. Natl. Acad.
1081   Sci. U.S.A., 111, 2915–2919, https://doi.org/10.1073/pnas.1315126111, 2014.

1082
1083 Pingali, P. L.: Green, Revolution: Impacts, limits, and the path ahead, Proc. Natl. Acad. Sci.
1084   U.S.A., 109, 12302–12308, https://doi.org/10.1073/pnas.0912953109, 2012.

1085
1086 Pongratz, J., Raddatz, T., Reick, C. H., Esch, M., and Claussen, M.: Radiative forcing from
1087   anthropogenic land cover change since A.D. 800, Geophys. Res. Lett., 36, L02709,
1088   https://doi.org/10.1029/2008GL036394, 2009.

1089
1090 Ramanathan, V.: Greenhouse Effect Due to Chlorofluorocarbons: Climatic Implications,
1091   Science, 190, 50–52, https://doi.org/10.1126/science.190.4209.50, 1975.

1092
1093 Sherwood, S. C., Bony, S., Boucher, O., Bretherton, C., Forster, P. M., Gregory, J. M., and
1094   Stevens, B.: Adjustments in the Forcing-Feedback Framework for Understanding Climate
1095   Change, Bull. Amer. Meteor. Soc., 96, 217–228, https://doi.org/10.1175/BAMS-D-13-
1096   00167.1, 2015.

1097
1098 Spawn, S. A., Lark, T. J., and Gibbs, H. K.: Carbon emissions from cropland expansion in the
1099   United States, Environ. Res. Lett., 14, 045009, https://doi.org/10.1088/1748-9326/ab0399,
1100   2019.

1101
1102 State Forestry Administration of the People's Republic of China Seventh National Forest
1103   Resource Inventory Report (2004-2008), (State Forestry Administration of the People's
1104   Republic of China, Beijing), 2009.

1105
1106 Stibig, H. J., Achard, F., Carboni, S., Raši, R., and Miettinen, J.: Change in tropical forest
1107   cover of Southeast Asia from 1990 to 2010, Biogeosciences, 11, 247–258,
1108   https://doi.org/10.5194/bg-11-247-2014, 2014.

1109
1110 Sun, W., Ding, X., Su, J., Mu, X., Zhang, Y., Gao, P., and Zhao, G.: Land use and cover
1111   changes on the Loess Plateau: A comparison of six global or national land use and cover
1112   datasets, Land Use Policy, 119, 106165, https://doi.org/10.1016/j.landusepol.2022.106165,
1113   2022.
1114

Teluguntla, P. G., Thenkabail, P. S., Xiong, J., Gumma, M. K., Giri, C., Milesi, C., Ozdogan, M., Congalton, R., Tilton, J., Sankey, T. T., Massey, R., Phalke, A., and Yadav, K.: Global Cropland Area Database (GCAD) derived from remote sensing in support of food security in the twenty-fifirst century: Current achievements and future possibilities, In P. S. Thenkabail (Ed.), Remote sensing handbook. Volume II, Land resources monitoring, modeling, and mapping with remote sensing (Chap. 7, p. 849), Chapter 7. Boca Raton: CRC Press, 2015.

Vose, R. S., Kari, T. R., Easterling, D. R., Williams, C. N., and Menne, M. J.: Impact of land-use change on climate, Nature, 427, 213–214, https://doi.org/10.1038/427213b, 2004.

Wang, X. M., Ge, Q. S., Geng, X., Wang, Z. S., Gao, L., Bryan, B. A., Chen, S. Q., Su, Y. N., Cai, D. W., Ye, J. S., Sun, J. M., Lu, H. Y., Liu, B. L., Dong, Z. B., Cao, S. X., Hua, T., Chen, S. Y., Sun, F. B., Luo, G. P., Wang, Z. T., Hu, S., Xu, D. Y., Chen, M. X., Li, D. F., Liu, F., Xu, X. L., Han, D. M., Zheng, Y., Xiao, F. Y., Li, X. B., Wang, P., and Chen, F. H.: Unintended consequences of combating desertification in China, Nat. Commun., 14, 1139, https://doi.org/10.1038/s41467-023-36835-z, 2023.

Ward, D. S., Mahowald, N. M., and Kloster, S.: Potential climate forcing of land use and land cover change, Atmos. Chem. Phys., 14, 12701–12724, https://doi:10.5194/acp-14-12701-2014, 2014.

Winkler, K., Fuchs, R., Rounsevell, M., and Herold, M.: Global land use changes are four times greater than previously estimated, Nat. Commun., 12, 2501, https://doi.org/10.1038/s41467-021-22702-2, 2021.

Yang, J. X.: China's Rapid Urbanization, Science, 342, 310–310, https://doi.org/10.1126/science.342.6156.310-a, 2013.

Zablon, A. A., Paolo, N., Vitaly, Z., and David, W.: Impact of grassland conversion to forest on groundwater recharge in the Nebraska Sand Hills, J. Hydrol. Reg. Stud., 15, 171–183, https://doi.org/10.1016/j.ejrh.2018.01.001, 2018.

Zhang, X. D., Huang, T., Zhang, L. M., Shen, Y. J., Zhao, Y., Gao, H., Mao, X. X., Jia, C. H., and Ma, J. M.: Three-North Shelter Forest Program contribution to long-term increasing trends of biogenic isoprene emissions in northern China, Atmos. Chem. Phys., 16, 6949–6960, https://doi.org/10.5194/acp-16-6949-2016, 2016.

Zhang, X. D., Huang, T., Zhang, L. M., Gao, H., Shen, Y. J., and Ma, J. M.: Trends of deposition fluxes and loadings of sulfur dioxide and nitrogen oxides in the artificial Three Northern Regions Shelter Forest across northern China, Environ. Pollut., 207, 238–247, https://doi.org/10.1016/j.envpol.2015.09.022, 2015.

Zhu, F., Emile-Geay, J., Mckay, N. P., Hakim, G. J., Khider, D., Ault, T. R., Steig, E. J., Dee, S., and Kirchner, J. W.: Cliamte models can correctly simulate the continuum of global-average temperature variability, Proc. Natl. Acad. Sci. U.S.A., 116, 8728–8733,

1161   https://doi.org/10.1073/pnas.1809959116, 2019.
1162